

# A motor cortex circuit for motor planning and movement

Nuo Li<sup>1</sup>, Tsai-Wen Chen<sup>1</sup>, Zengcui V. Guo<sup>1</sup>, Charles R. Gerfen<sup>2</sup> & Karel Svoboda<sup>1</sup>

**Activity in motor cortex predicts specific movements seconds before they occur, but how this preparatory activity relates to upcoming movements is obscure. We dissected the conversion of preparatory activity to movement within a structured motor cortex circuit. An anterior lateral region of the mouse cortex (a possible homologue of premotor cortex in primates) contains equal proportions of intermingled neurons predicting ipsi- or contralateral movements, yet unilateral inactivation of this cortical region during movement planning disrupts contralateral movements. Using cell-type-specific electrophysiology, cellular imaging and optogenetic perturbation, we show that layer 5 neurons projecting within the cortex have unbiased laterality. Activity with a contralateral population bias arises specifically in layer 5 neurons projecting to the brainstem, and only late during movement planning. These results reveal the transformation of distributed preparatory activity into movement commands within hierarchically organized cortical circuits.**

The motor cortex is critical for planning and the execution of voluntary movements<sup>1</sup>. Unilateral lesions in premotor areas of motor cortex disrupt planning of movements into the contra-lesional space<sup>2–4</sup>. Neurons in premotor cortex have activity anticipating specific movements long before movement onset<sup>1,5–8</sup>, a neural correlate of movement planning<sup>1</sup>. But intermingled motor cortex neurons show puzzlingly diverse selectivity<sup>9,10</sup> for multiple movement directions with complex dynamics<sup>4,11,12</sup>. The relationship of this complex preparatory activity to future movements is not understood. A key question is how preparatory activity evolves into commands that descend to motor centres to trigger movement.

In the mouse, the anterior lateral motor cortex (ALM) is involved in planning directed licking<sup>13</sup>. Unilateral inactivation of ALM during movement planning interferes with upcoming tongue movements in the contralateral direction without impairing movements<sup>13</sup>. A large proportion of ALM neurons exhibit preparatory activity that predicts movements<sup>13</sup>, similar to premotor cortex in non-human primates<sup>1,7,8,11,14</sup>. Despite the lateralized deficit from ALM inactivation, ALM neurons in each hemisphere have a preference for contra- or ipsilateral movements in roughly equal proportions<sup>13</sup>.

To determine how silencing a brain area with non-lateralized selectivity causes a directional movement bias we measured neuronal activity within hierarchically organized ALM circuits. ALM projection neurons include two major classes: intratelencephalic neurons that project to other cortical areas and pyramidal tract neurons that project out of the cortex, including to motor-related areas in the brainstem<sup>15,16</sup>. Intratelencephalic neurons connect to other intratelencephalic neurons and excite pyramidal tract neurons, but not vice versa. Pyramidal tract neurons are thus at the output end of the local ALM circuit<sup>16–19</sup>. We show that equal proportions of intratelencephalic neurons have preparatory activity for either ipsi- or contralateral movements. Contralateral population activity in pyramidal tract neurons arises late during movement planning to drive directional licking. Our results reveal the flow of information within motor cortex circuits involved in converting preparatory activity into movements.

## ALM is required for movement planning

We tested head-fixed mice ( $n = 42$ ) in a whisker-based object location discrimination task<sup>13,20,21</sup>. In each trial, a vertical pole was presented in one of two positions (anterior or posterior) during a sample epoch (1.3 s)

(Fig. 1a, b). Mice discriminated pole location using their whiskers. During a subsequent delay epoch (1.3 s) mice planned the upcoming response. An auditory ‘go’ cue (0.1 s) signalled the beginning of the response epoch, when mice reported the perceived pole position by licking one of two ‘lickports’ (posterior, lick right; anterior, lick left) (mean per cent correct, 78.4%; responses before the go cue, ~13%).

Unilateral photoinhibition (Methods) of anterior lateral motor cortex (ALM, centred at 2.5 mm anterior, 1.5 mm lateral), limited to the delay epoch, produced an ipsilateral bias (Fig. 1c, d)<sup>13</sup>. Inhibiting left ALM caused a tendency to lick the left port, resulting in increased performance in ‘lick left’ trials and decreased performance in ‘lick right’ trials (Fig. 1d). The reversed pattern of bias was observed when inhibiting right ALM. This ipsilateral bias was smaller when photoinhibiting during the sample epoch. ALM activity during the delay period is required for movement planning.

## ALM contains neurons with bilateral selectivity

We recorded single units ( $n = 1,408$ ; 19 mice) from left ALM in mice performing object location discrimination. Here we focus on putative pyramidal neurons (Extended Data Fig. 1;  $n = 1,245$ , Methods) because they carry signals out of the motor cortex to cause movements. A large fraction (73%, 912/1,245) of neurons distinguished trial types ( $P < 0.05$ , two-tailed *t*-test, not corrected for multiple comparisons) (Fig. 2b)<sup>13</sup>. Selectivity emerged in the sample epoch, increased throughout the delay epoch, and reached a maximum at the beginning of the response epoch (Fig. 2c and Extended Data Fig. 1d, f). Individual neuron responses were dynamic, despite stable selectivity at the level of the population (Fig. 2c, bottom panel and Extended Data Fig. 2a). ALM neuron responses were diverse: subsets of neurons showed selective preparatory activity (Fig. 2b, left column; Fig. 2d, 219/912 neurons), peri-movement activity during the response epoch (Fig. 2b, right column; 389/912), or both (Fig. 2b, middle column; 304/912). On error trials, when mice licked in the opposite direction to the instruction provided by object location (Fig. 1a), neuronal activity predicted the licking direction (Extended Data Fig. 2b, c)<sup>13</sup>. Such choice-specific activity is consistent with a role in planning and driving movements.

Unilateral inactivation of preparatory activity during the delay epoch caused an ipsilateral bias (contra-lesional deficit) in the upcoming

<sup>1</sup>Janelia Research Campus, Howard Hughes Medical Institute, Ashburn, Virginia 20147, USA. <sup>2</sup>Laboratory of Systems Neuroscience, National Institute of Mental Health, Bethesda, Maryland 20892, USA.

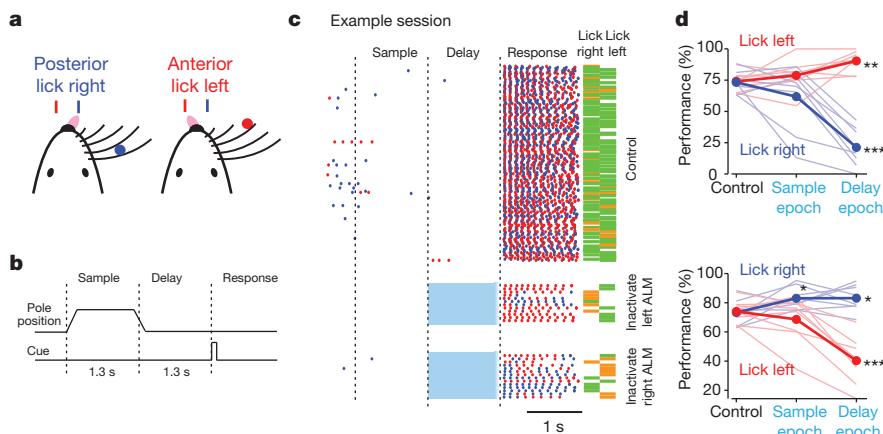


**Figure 1 | ALM is required for movement planning.** **a**, Head-fixed mouse responding lick right or lick left based on pole location. **b**, The pole was within reach during the sample epoch. Mice responded with licking after a delay and an auditory go cue. **c**, Behavioural data. Individual licks, dots (blue, lick right; red, lick left). Right, bars indicate the performance (green, correct; orange, incorrect). Cyan region, photoinhibition. **d**, Performance with photoinhibition of left (top) or right (bottom) ALM during different trial epochs. Thick lines, mean; thin lines, individual mice ( $n = 8$ ). \* $P < 0.05$ ; \*\* $P < 0.01$ ; \*\*\* $P < 0.001$ ; one-tailed test, bootstrap (Methods).

movement (Fig. 1d). This suggests that ALM neurons have lateralized preference for contralateral movements (that is, neurons from left ALM respond more during lick right trials). We categorized individual neurons as ‘contra-preferring’ or ‘ipsi-preferring’ based on spike counts across the trial epochs. Paradoxically, this simple measure did not detect a preference for contralateral licking in ALM spike rates (Fig. 2c, e).

Significant contralateral bias also did not appear in the overall spike count across the recorded population of neurons (Extended Data Fig. 1;  $P = 0.13$ , two-tailed  $t$ -test against 0). Individual neurons were either contra-selective (Fig. 2b, top row), or ipsi-selective (Fig. 2b, middle row), or showed mixed selectivity (Fig. 2b, bottom row). The contra-preferring and ipsi-preferring neurons were present in equal proportions (Fig. 2c, e).

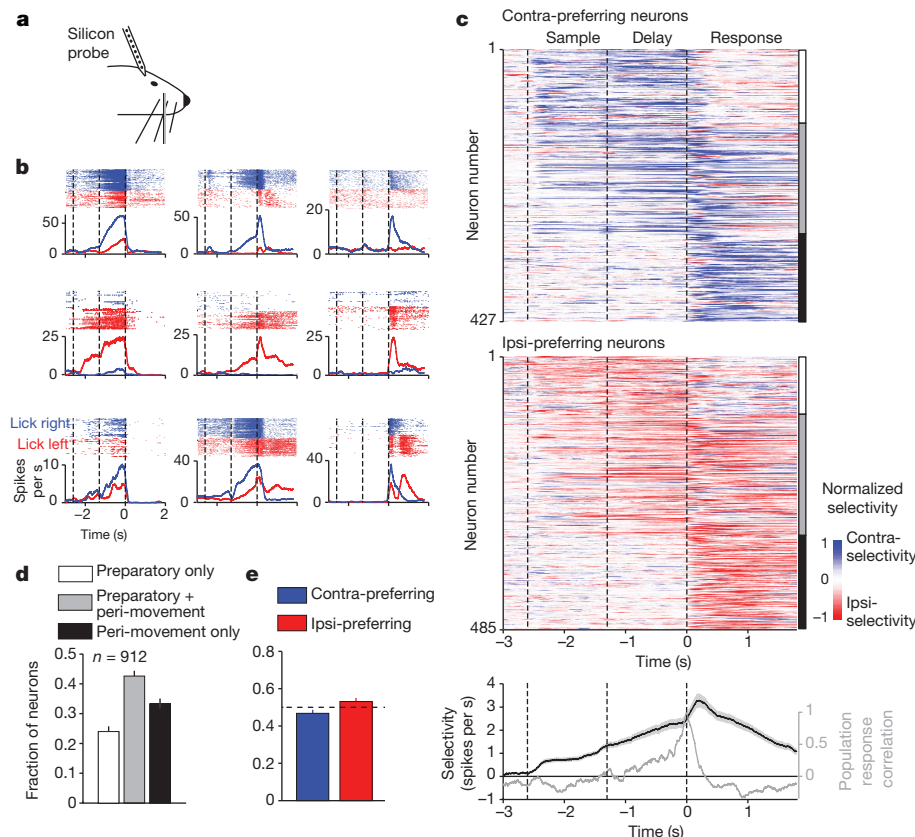


**Figure 2 | ALM contains neurons with bilateral movement selectivity.**

**a**, Silicon probe recordings. **b**, Peri-stimulus time histograms of nine example ALM neurons. Correct lick right (blue) and lick left (red) trials only. Dashed lines, behavioural epochs. **c**, ALM population selectivity. Top, selectivity is the difference in spike rate between the preferred and non-preferred trial type, normalized to the peak selectivity (Methods). Only putative pyramidal neurons with significant trial selectivity are shown ( $n = 912/1,245$ ). Bottom, average

population selectivity in spike rate (black line,  $\pm$ s.e.m. across neurons, bootstrap) and population response correlation (grey line; Pearson’s correlation between the population response at a particular time and the population response at the onset of the go cue.  $t = 0$ ; Methods). Averaging window, 200 ms. **d**, Proportion of neurons with preparatory and peri-movement activity. **e**, Proportion of contra-preferring versus ipsi-preferring neurons. Error bars, s.e.m. across mice, bootstrap.

## Pyramidal tract neurons control directional licking

Selectivity may be distributed non-uniformly across cortical cell types. ALM is interconnected with other cortical areas, including the contralateral ALM (via the corpus callosum), by intratelencephalic neurons (Extended Data Fig. 3a). Intratelencephalic neurons also target ipsi- and contralateral striatum, but avoid subcortical structures involved in the control of movements (Extended Data Fig. 4). Pyramidal tract neurons in layer 5B project to subcortical structures that control movement, including the superior colliculus, brainstem and spinal cord. Pyramidal tract neurons in ALM project to the contralateral intermediate nucleus of the reticular formation, which is presynaptic to the hypoglossal nucleus and the intrinsic and extrinsic muscles of the tongue (Extended Data Fig. 3b, c)<sup>22,23</sup>. Injection of retrograde tracers in the ipsilateral pontine nucleus and the contralateral ALM labelled non-overlapping populations of intratelencephalic neurons and pyramidal tract neurons (Extended Data Fig. 3d) (doubly labelled neurons, <4%, n = 2 mice). Intratelencephalic and pyramidal tract neurons were spatially intermingled in

layer 5B, but intratelencephalic neurons were also found in superficial layers.

We expressed ChR2 selectively in intratelencephalic or pyramidal tract neurons (Extended Data Fig. 4). Unilateral photostimulation of ALM intratelencephalic or pyramidal tract neurons ('high' power, 0.8 mW, 2 ms pulses at 20 Hz, Methods) triggered contralateral licking with short latencies (Extended Data Fig. 3e), even in untrained mice (Extended Data Fig. 3f)<sup>15,24–26</sup>. This is consistent with the crossed pyramidal tract projection to the brainstem (Extended Data Fig. 3a) and the observation that stimulation of one hypoglossal nerve causes tongue movements in the ipsilateral direction<sup>27</sup>. Photostimulating the vibrissal motor cortex (anterior 1 mm, lateral 1 mm) caused whisker protraction but not licking (Extended Data Fig. 3e–g)<sup>24–26</sup>. Similarly, in mice performing object location discrimination high-power photostimulation of either intratelencephalic or pyramidal tract neurons in ALM produced premature licking in the contralateral direction (Extended Data Fig. 3e). This observation shows that lateralized licking can be triggered by population

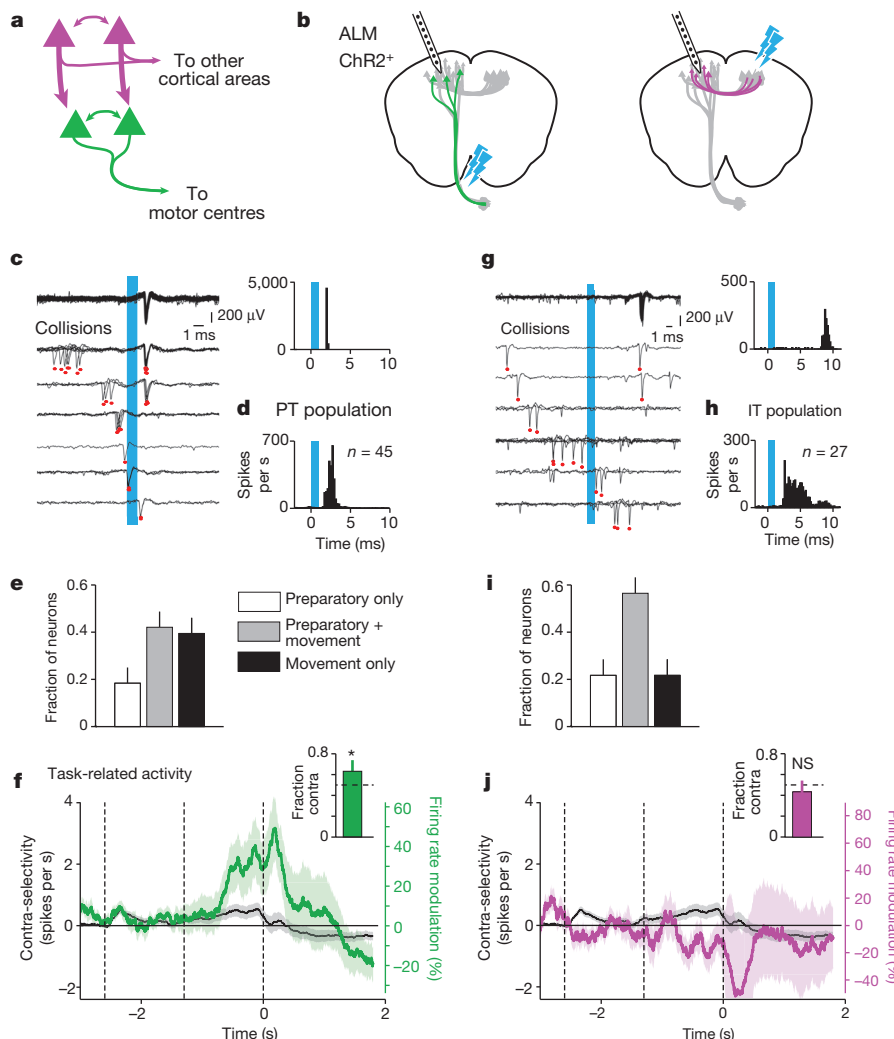


**Figure 3 | Cell-type-specific electrophysiology.** **a**, ALM circuit involving pyramidal tract (green) and intratelencephalic (magenta) neurons. **b**, Cell-type-specific recordings. Cyan arrows, photostimulation. **c**, Left, recordings from an example pyramidal tract neuron during photostimulation (cyan bar) with collisions. As spontaneous spikes occurred closer in time to the light stimulus, the probability of observing a light-evoked spike decreased (top to bottom traces). Red ticks, individual spikes. Right, peri-stimulus time histogram shows the light-evoked response for the pyramidal tract neuron. **d**, Light-evoked response across all pyramidal tract (PT) neurons ( $n = 45$ ). **e**, Fraction of

pyramidal tract neurons sorted by preparatory vs. peri-movement activity. **f**, Contra-selectivity across all pyramidal tract neurons (green, mean  $\pm$  s.e.m.) and all task-selective neurons (black). Contra-selectivity is the spike rate difference between lick right and light left trials. Insert, fraction of contra-prefering pyramidal tract neurons. \* $P < 0.05$ , significantly more contra-prefering neurons than ipsi-prefering neurons, one-tailed test, bootstrap. **g–j**, Same as **c–f** for intratelencephalic (IT) neurons. Error bars, s.e.m. across animals, bootstrap.

activity arising in contralateral ALM pyramidal tract neurons. Stimulation of intratelencephalic neurons is also expected to cause lateralized licking because intratelencephalic neurons locally excite pyramidal tract neurons<sup>17</sup>.

### A movement command emerges in the pyramidal tract neurons

We next recorded selectively from ChR2-expressing intratelencephalic or pyramidal tract neurons during behaviour. During extracellular recordings in left ALM we searched for neurons antidromically activated by photostimulating ('tagging') axonal sites in the pons (pyramidal tract) or contralateral ALM (intratelencephalic)<sup>28</sup> (Methods, Fig. 3b and Extended Data Fig. 5a, c). Photostimulation triggered action potentials in ALM, with short latency and sub-millisecond temporal jitter (mean, 0.15 ms) (Fig. 3c, g and Extended Data Fig. 5b, d). To exclude indirectly activated neurons we tested for collisions between action potentials

triggered by axonal photostimulation and somatic action potentials (Methods, Fig. 3c, g and Extended Data Fig. 5b, d)<sup>29,30</sup>. In total, 45 pyramidal tract neurons and 27 intratelencephalic neurons passed the collision test (out of 1,408 neurons recorded in 19 mice) (Methods, Extended Data Fig. 5f). Pyramidal tract neurons had shorter latencies than intratelencephalic neurons (pyramidal tract mean, 2.7 ms; intratelencephalic mean, 4.6 ms) (Extended Data Fig. 5e)<sup>6,31</sup>.

Both intratelencephalic and pyramidal tract neurons displayed preparatory and movement-related activity (Fig. 3e, i)<sup>5,6,31</sup>. Contra-preferring neurons outnumbered ipsi-preferring neurons for the pyramidal tract neurons (Fig. 3f;  $P < 0.05$ , bootstrap, Methods), but not the intratelencephalic neurons (Fig. 3j,  $P = 0.74$ ). Robust contralateral selectivity (the spike count difference for lick right trials and lick left trials) emerged in pyramidal tract neuron responses starting 570 ms before the response epoch (Fig. 3f; 34% spike rate modulation;  $P < 0.05$ , two-tailed  $t$ -test against 0 in spike counts), but not for intratelencephalic neurons ( $-19\%$

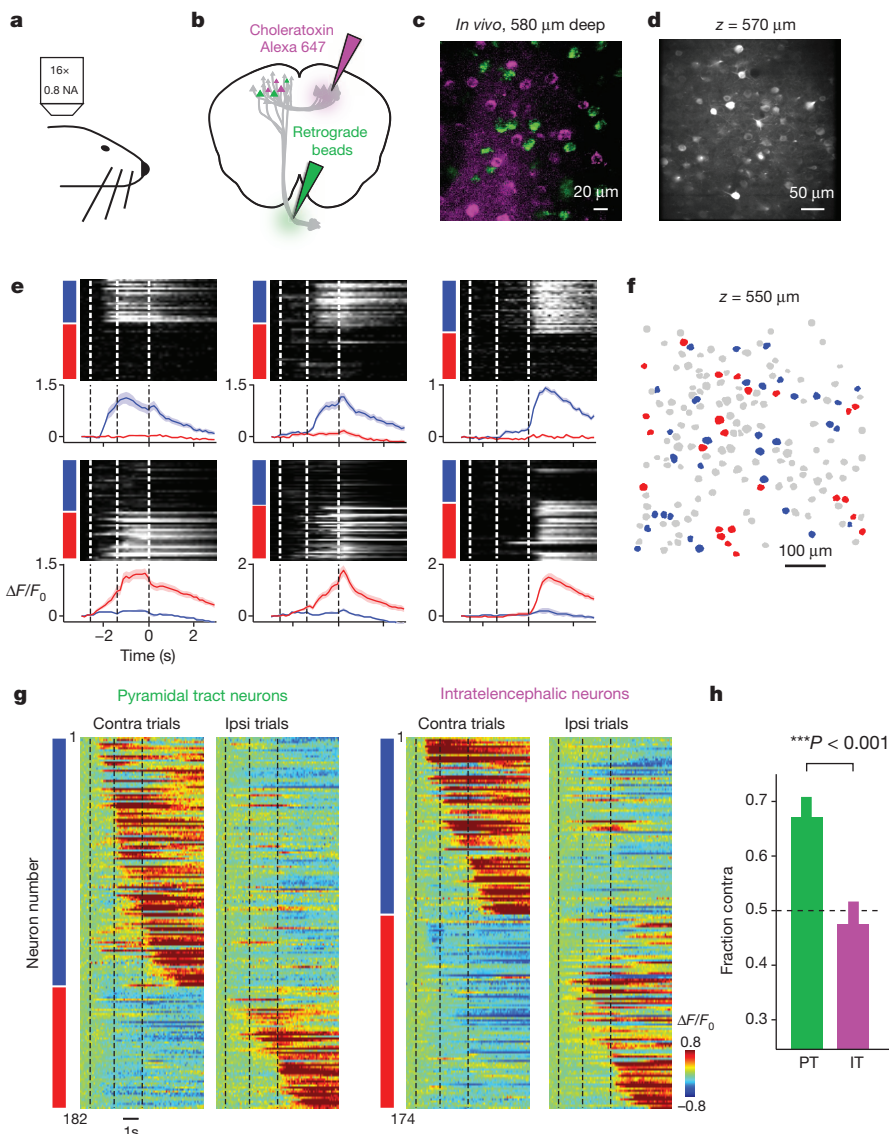


**Figure 4 | Cell-type-specific imaging.** **a**, Two-photon microscopy. **b**, Labelling pyramidal tract neurons (green) and intratelencephalic neurons (magenta). **c**, Example imaging plane. **d**, Layer 5 neurons expressing GCaMP6s. **e**, Six example ALM neurons. Top, normalized  $\Delta F/F_0$  across multiple trials. Coloured bars, trial type (blue, lick right trials; red, lick left trials). Bottom,  $\Delta F/F_0$ , mean and s.e.m. Dashed lines, behavioural epochs. **f**, Contra-preferring neurons (blue) and ipsi-preferring layer 5 neurons (red) in an example field of view. Grey, non-selective (Methods). **g**, Left, average  $\Delta F/F_0$  for selective

pyramidal tract neurons. Right, intratelencephalic neurons. Neurons are sorted by their preference (left bar); blue, contra-preferring; red, ipsi-preferring. **h**, Fraction of contra-preferring neurons. Pyramidal tract (PT) neurons were more likely to be contra-preferring than ipsi-preferring ( $P < 0.001$ , binomial test), but not intratelencephalic (IT) neurons ( $P > 0.05$ ). Pyramidal tract neurons were more likely to be contra-preferring compared to intratelencephalic neurons ( $P < 0.001$ ,  $\chi^2$  test). Error bars, s.e.m. across neurons, bootstrap.

spike rate modulation;  $P = 0.40$ ) nor for all task-selective neurons (8% spike rate modulation;  $P = 0.13$ ) (Fig. 3j). Contralateral population selectivity thus arises selectively in pyramidal tract neurons hundreds of milliseconds before movement.

Two-photon calcium imaging provided a much larger sample of pyramidal tract and intratelencephalic neurons. Pyramidal neurons in the left ALM were labelled with GCaMP6s<sup>32</sup>, in addition subsets of pyramidal tract and intratelencephalic neurons were labelled with retrograde fluorescent markers (Methods, Fig. 4b, c)<sup>33,34</sup>. We imaged randomly selected fields of view in ALM (size, 400–600  $\mu\text{m}$ ; 59 fields of view;  $n = 4$  mice) (Fig. 4d; Methods). Consistent with single-unit recordings, imaging revealed neurons activated at different times during the task (Fig. 4e). We categorized selective neurons into contra-preferring or ipsi-preferring, based on their average calcium signal during the trial epochs (Fig. 4e). Contra-preferring and ipsi-preferring neurons were observed in all fields of view (Fig. 4f; Methods). The probability that nearby neurons share the same selectivity was not different from randomized data ( $P = 0.34$ , bootstrap, Methods). The distance between nearest neurons with the same selectivity was also not different from chance ( $P = 0.61$ , bootstrap). Contra-preferring and ipsi-preferring neurons were thus spatially intermingled.

We next analysed pyramidal tract ( $n = 534$ ) and intratelencephalic ( $n = 542$ ) neurons in layer 5 (imaging depth 450–700  $\mu\text{m}$ ;  $n = 4$  mice) (Fig. 4g). Approximately a quarter of the labelled pyramidal tract (182/534) and intratelencephalic (174/542) neurons were selective (Methods). Consistent with electrophysiological tagging (Fig. 3), we observed more contra-preferring than ipsi-preferring neurons in the pyramidal tract neuron population (67%, 122/182, Fig. 4g, h;  $P < 0.001$ , binomial test), but not in the intratelencephalic neurons (fraction of contra-preferring neurons: 48%, 83/174; Fig. 4g, h). Contra-lateral preference thus emerges in populations of pyramidal tract neurons.

## Pyramidal tract neurons drive upcoming movements

Cell-type-specific recordings revealed that a contralateral selective population signal emerges in pyramidal tract neurons late in the delay epoch, before movement onset (Fig. 3f, selectivity onset: 570 ms before cue; reaction time post cue onset across mice:  $61.1 \pm 10.5$  ms, mean  $\pm$  s.d.). This suggests that the contra-preferring population activity in pyramidal tract neurons drives the upcoming contralateral licking. We tested this hypothesis directly by activating pyramidal tract neurons during the delay epoch.

We attenuated photostimuli below threshold for activating movement during the sample or delay epochs ('subthreshold' power,  $<0.25$  mW, 2 ms pulses, 20 Hz). Photostimulation was deployed on 25% of the trials either during the sample or delay epochs and ended before the response cue (Methods). Subthreshold photostimulation of the pyramidal tract neurons during the delay epoch biased licking to the contralateral direction. Subthreshold stimulation of pyramidal tract neurons in the left ALM produced a rightward bias, resulting in a decrease in performance in the lick left trials and vice versa (Fig. 5). The effect size was monotonically dependent on laser power (Extended Data Fig. 6b).

Notably, stimulation of pyramidal tract neurons during the sample epoch also caused a significant contralateral bias (Fig. 5b). Simultaneous recordings and optogenetics revealed that subthreshold stimulation of pyramidal tract neurons caused changes in ALM activity and a directional bias that persisted for seconds after cessation of the photostimulus (Extended Data Fig. 7). Activating pyramidal tract neurons is thus sufficient to generate preparatory activity and bias future movements.

Subthreshold photostimulation of the intratelencephalic neurons also caused behavioural changes, but these varied across mice and depended non-monotonically on laser intensity (Extended Data Fig. 6d). This unpredictable and inconsistent effect of intratelencephalic neuron activation on licking direction could be related to the intermingled contralateral and ipsilateral selectivity found in intratelencephalic neurons (Figs 3 and 4). Photostimuli with different powers and in different animals will activate random subsets of intratelencephalic neurons with random net

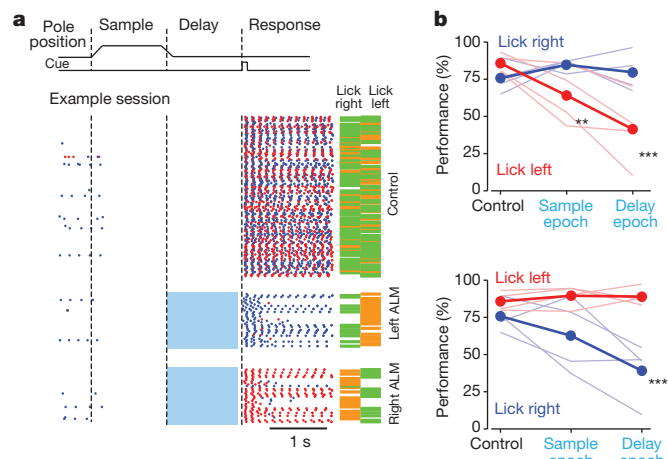


**Figure 5 | Preparatory activity in pyramidal tract neurons drives upcoming movements.** a, Top, trial structure. Bottom, data from one example session with pyramidal tract neuron activation in the delay epoch. Colour code as Fig. 1c. b, Performance in control trials and with pyramidal tract neuron photostimulation in different trial epochs. Top, photostimulation in left ALM. Bottom, right ALM. Colour code as Fig. 1d. \*\* $P < 0.01$ ; \*\*\* $P < 0.001$ ; one-tailed test, bootstrap (Methods). Photostimulation data with multiple subthreshold laser intensities were pooled (0.12–0.8 mW). See Extended Data Fig. 6 for dose response.

selectivity; the resulting network activity will evolve over time to cause unpredictable effects on behaviour (Fig. 2c).

## Discussion

Unilateral silencing of ALM during the delay epoch biases future movements in the ipsilateral direction (Fig. 1). ALM also contains a large fraction of neurons with preparatory activity, predicting upcoming movements (Fig. 2)<sup>13</sup>, similar to primate premotor cortex<sup>1,5,7,8</sup>. These functional data as well as anatomical studies<sup>35,36</sup> suggest that ALM is homologous to premotor cortex in non-human primates. ALM overlaps with rostral forelimb area, a previously defined premotor region in rats involved in the control of limb movement<sup>36</sup>. Although we studied ALM in the context of licking, ALM and nearby motor cortical areas also have roles in planning other movements<sup>4,37,38</sup> (unpublished data).

Preparatory activity is not an attenuated form of peri-movement activity, but evolves with complex dynamics<sup>1</sup> (Fig. 2b, c and Extended Data Fig. 2a). Lateralized licking is driven by contralateral population activity in populations of pyramidal tract neurons in ALM (Figs 3, 4 and Extended Data Fig. 3). Pyramidal tract neurons are downstream of intratelencephalic neurons, which show contralateral and ipsilateral selectivity with little contralateral bias. This suggests that during movement planning distributed preparatory activity in intratelencephalic neuron networks is converted into a movement command in pyramidal tract neurons ('output-potent' activity)<sup>39</sup>, which ultimately triggers directional movements.

Contralateral population activity in pyramidal tract neuron populations still appears hundreds of milliseconds before movement onset (Fig. 3f). Why this pyramidal tract neuron activity, the presumed motor command, does not cause early movements is not understood. One possibility is that a disinhibitory signal from the basal ganglia<sup>40</sup>, triggered by the go cue<sup>41</sup>, may be necessary to release brainstem motor programs. The same signal could also be routed into ALM through the motor thalamus to reorganize pyramidal tract neuron activity further to make it even more potent for triggering movement<sup>39</sup>.

Similar to ALM, human premotor cortex shows bilateral symmetric preparatory potentials (Bereitschaftspotential)<sup>42</sup>. Bilateral coding of movement directions has been observed in single-unit recordings from primate<sup>11,12,43</sup> and rat motor cortex<sup>4</sup>. In contrast to the bilateral selectivity in neurons, unilateral damage to the premotor cortices frequently

causes hemi-neglect, where subjects show deficit in planning movements to the contra-lesional space<sup>2–4</sup>. Our results suggest that the contra-lesional bias in premotor hemi-neglect is caused by damage to the pyramidal tract neurons.

**Online Content** Methods, along with any additional Extended Data display items and Source Data, are available in the online version of the paper; references unique to these sections appear only in the online paper.

Received 14 August; accepted 23 December 2014.

Published online 25 February 2015.

1. Shenoy, K. V., Sahani, M. & Churchland, M. M. Cortical control of arm movements: a dynamical systems perspective. *Annu. Rev. Neurosci.* **36**, 337–359 (2013).
2. Kerhoffer, G. Spatial hemineglect in humans. *Prog. Neurobiol.* **63**, 1–27 (2001).
3. Rizzolatti, G., Matelli, M. & Pavesi, G. Deficits in attention and movement following the removal of postarcuate (area 6) and prearcuate (area 8) cortex in macaque monkeys. *Brain* **106**, 655–673 (1983).
4. Erlich, J. C., Bialek, M. & Brody, C. D. A cortical substrate for memory-guided orienting in the rat. *Neuron* **72**, 330–343 (2011).
5. Tanji, J. & Evarts, E. V. Anticipatory activity of motor cortex neurons in relation to direction of an intended movement. *J. Neurophysiol.* **39**, 1062–1068 (1976).
6. Turner, R. S. & DeLong, M. R. Corticostriatal activity in primary motor cortex of the macaque. *J. Neurosci.* **20**, 7096–7108 (2000).
7. Crutcher, M. D. & Alexander, G. E. Movement-related neuronal activity selectively coding either direction or muscle pattern in three motor areas of the monkey. *J. Neurophysiol.* **64**, 151–163 (1990).
8. Riehle, A. & Requin, J. Monkey primary motor and premotor cortex: single-cell activity related to prior information about direction and extent of an intended movement. *J. Neurophysiol.* **61**, 534–549 (1989).
9. Scott, S. H. Inconvenient truths about neural processing in primary motor cortex. *J. Physiol. (Lond.)* **586**, 1217–1224 (2008).
10. Huber, D. et al. Multiple dynamic representations in the motor cortex during sensorimotor learning. *Nature* **484**, 473–478 (2012).
11. Rizzolatti, G. et al. Functional organization of inferior area 6 in the macaque monkey. II. Area F5 and the control of distal movements. *Exp. Brain Res.* **71**, 491–507 (1988).
12. Arce, F. I., Lee, J. C., Ross, C. F., Sessle, B. J. & Hatsopoulos, N. G. Directional information from neuronal ensembles in the primate orofacial sensorimotor cortex. *J. Neurophysiol.* **110**, 1357–1369 (2013).
13. Guo, Z. V. et al. Flow of cortical activity underlying a tactile decision in mice. *Neuron* **81**, 179–194 (2014).
14. Bruce, C. J. & Goldberg, M. E. Primate frontal eye fields. I. Single neurons discharging before saccades. *J. Neurophysiol.* **53**, 603–635 (1985).
15. Komiyama, T. et al. Learning-related fine-scale specificity imaged in motor cortex circuits of behaving mice. *Nature* **464**, 1182–1186 (2010).
16. Shepherd, G. M. Corticostriatal connectivity and its role in disease. *Nature Rev. Neurosci.* **14**, 278–291 (2013).
17. Kiritani, T., Wickersham, I. R., Seung, H. S. & Shepherd, G. M. Hierarchical connectivity and connection-specific dynamics in the corticospinal-corticostriatal microcircuit in mouse motor cortex. *J. Neurosci.* **32**, 4992–5001 (2012).
18. Brown, S. P. & Hestrin, S. Intracortical circuits of pyramidal neurons reflect their long-range axonal targets. *Nature* **457**, 1133–1136 (2009).
19. Morishima, M. & Kawaguchi, Y. Recurrent connection patterns of corticostriatal pyramidal cells in frontal cortex. *J. Neurosci.* **26**, 4394–4405 (2006).
20. O'Connor, D. H. et al. Vibrissa-based object localization in head-fixed mice. *J. Neurosci.* **30**, 1947–1967 (2010).
21. Guo, Z. V. et al. Procedures for behavioral experiments in head-fixed mice. *PLoS ONE* **9**, e88678 (2014).
22. Travers, J. B., Dinardo, L. A. & Karimnamazi, H. Motor and premotor mechanisms of licking. *Neurosci. Biobehav. Rev.* **21**, 631–647 (1997).
23. Stanek, E. t., Cheng, S., Takatoh, J., Han, B. X. & Wang, F. Monosynaptic premotor circuit tracing reveals neural substrates for oro-motor coordination. *eLife* **3**, e02511 (2014).
24. Li, C. X. & Waters, R. S. Organization of the mouse motor cortex studied by retrograde tracing and intracortical microstimulation (ICMS) mapping. *Can. J. Neurol. Sci.* **18**, 28–38 (1991).
25. Hall, R. D. & Lindholm, E. P. Organization of motor and somatosensory neocortex in the albino rat. *Brain Res.* **66**, 23–38 (1974).
26. Neafsey, E. J. et al. The organization of the rat motor cortex: a microstimulation mapping study. *Brain Res.* **396**, 77–96 (1986).
27. Bennett, G. A. & Ramsay, A. J. Experimental studies on the movements of the mammalian tongue. I. Movements of the split tongue (dog). *Anat. Rec.* **79**, 39–51 (1941).
28. Petreanu, L., Huber, D., Sobczyk, A. & Svoboda, K. Channelrhodopsin-2-assisted circuit mapping of long-range callosal projections. *Nature Neurosci.* **10**, 663–668 (2007).
29. Beloozerova, I. N., Sirota, M. G. & Swadlow, H. A. Activity of different classes of neurons of the motor cortex during locomotion. *J. Neurosci.* **23**, 1087–1097 (2003).
30. Swadlow, H. A. Efferent neurons and suspected interneurons in motor cortex of the awake rabbit: axonal properties, sensory receptive fields, and subthreshold synaptic inputs. *J. Neurophysiol.* **71**, 437–453 (1994).
31. Bauswein, E., Fromm, C. & Preuss, A. Corticostriatal cells in comparison with pyramidal tract neurons: contrasting properties in the behaving monkey. *Brain Res.* **493**, 198–203 (1989).
32. Chen, T. W. et al. Ultrasensitive fluorescent proteins for imaging neuronal activity. *Nature* **499**, 295–300 (2013).
33. Sato, T. R. & Svoboda, K. The functional properties of barrel cortex neurons projecting to the primary motor cortex. *J. Neurosci.* **30**, 4256–4260 (2010).
34. Yamashita, T. et al. Membrane potential dynamics of neocortical projection neurons driving target-specific signals. *Neuron* **80**, 1477–1490 (2013).
35. Reep, R. L., Corwin, J. V., Hashimoto, A. & Watson, R. T. Efferent connections of the rostral portion of medial agranular cortex in rats. *Brain Res. Bull.* **19**, 203–221 (1987).
36. Rouiller, E. M., Moret, V. & Liang, F. Comparison of the connectional properties of the two forelimb areas of the rat sensorimotor cortex: support for the presence of a premotor or supplementary motor cortical area. *Somatosens. Mot. Res.* **10**, 269–289 (1993).
37. Murakami, M., Vicente, M. I., Costa, G. M. & Mainen, Z. F. Neural antecedents of self-initiated actions in secondary motor cortex. *Nature Neurosci.* **17**, 1574–1582 (2014).
38. Sul, J. H., Jo, S., Lee, D. & Jung, M. W. Role of rodent secondary motor cortex in value-based action selection. *Nature Neurosci.* **14**, 1202–1208 (2011).
39. Kaufman, M. T., Churchland, M. M., Ryu, S. I. & Shenoy, K. V. Cortical activity in the null space: permitting preparation without movement. *Nature Neurosci.* **17**, 440–448 (2014).
40. Hikosaka, O. & Wurtz, R. H. Modification of saccadic eye movements by GABA-related substances. II. Effects of muscimol in monkey substantia nigra pars reticulata. *J. Neurophysiol.* **53**, 292–308 (1985).
41. Pan, W. X., Brown, J. & Dudman, J. T. Neural signals of extinction in the inhibitory microcircuit of the ventral midbrain. *Nature Neurosci.* **16**, 71–78 (2013).
42. Shibasaki, H. & Hallett, M. What is the Bereitschaftspotential? *Clin. Neurophysiol.* **117**, 2341–2356 (2006).
43. Murray, G. M. & Sessle, B. J. Functional properties of single neurons in the face primary motor cortex of the primate. III. Relations with different directions of trained tongue protrusion. *J. Neurophysiol.* **67**, 775–785 (1992).

**Acknowledgements** We thank B. Dickson, S. Druckmann, J. Dudman, D. Gutnisky, H. Inagaki, V. Jayaraman, D. O'Connor, S. Peron, T. Sato and G. Shepherd for comments on the manuscript and discussion, L. Walendy and E. Ophir for animal training, S. Michael and A. Hu for histology, T. Harris and B. Barbarits for the silicon probe recording system. This work was funded by the Howard Hughes Medical Institute. N.L. is a Helen Hay Whitney Foundation postdoctoral fellow.

**Author Contributions** N.L., Z.G. and K.S. initiated this study. N.L. performed electrophysiology and optogenetic experiments. T.W.C. performed imaging. T.W.C., N.L., and C.G. performed anatomical experiments. N.L., T.W.C., K.S. analysed data. N.L. and K.S. wrote the paper, with input from all authors.

**Author Information** Data have been deposited at <https://crcns.org/> and can be accessed at <http://dx.doi.org/10.6080/K0RF5RZT>. Reprints and permissions information is available at [www.nature.com/reprints](http://www.nature.com/reprints). The authors declare no competing financial interests. Readers are welcome to comment on the online version of the paper. Correspondence and requests for materials should be addressed to K.S. (svobodak@janelia.hhmi.org).

## METHODS

No statistical methods were used to predetermine sample size.

**Mice.** This study is based on data from 52 mice (age > P60). Five VGAT-ChR2-EYFP mice (Jackson laboratory, JAX Stock#014548)<sup>44</sup> and three PV-ires-Cre<sup>45</sup> crossed to Rosa26-LSL-ReaChR, red-shifted channelrhodopsin reporter mice (JAX 28846)<sup>46</sup>, were used for photoinhibition experiments (Fig. 1)<sup>13</sup>. Nine Sim1\_KJ18-Cre mice (MMRRC 031742), 3 Rbp4-Cre mice (MMRRC 031125), and 4 Tlx\_PL56-Cre mice (MMRRC 036547) were used for electrophysiology experiments (Figs 2 and 3)<sup>47</sup>. Four C57Bl/6Crl mice were used for imaging experiments (Fig. 4). Seven Sim1\_KJ18-Cre crossed to Ai32 (Rosa26-ChR2 reporter mice, JAX Stock#012569)<sup>48</sup> mice were used for photoactivation behavioural experiments (Fig. 5 and Extended Data Fig. 3), and one of these mice was also used for electrophysiology. Seven Tlx\_PL56-Cre crossed to Ai32 mice were used for photoactivation behaviour experiments and two of these mice were also used for electrophysiology. Two Sim1\_KJ18-Cre, 2 Tlx\_PL56-Cre, 4 C57Bl/6Crl mice, 1 Sim1\_KJ18-Cre × Ai32 mouse, and 1 Tlx\_PL56-Cre × Ai32 mouse were used for anatomy experiments (Extended Data Figs 3 and 4).

All procedures were in accordance with protocols approved by the Janelia Research Campus Institutional Animal Care and Use Committee. Mice were housed in a 12:12 reverse light:dark cycle and tested during the dark phase. On days not tested, mice received 1 ml of water. On other days, mice were tested in experimental sessions lasting 1 to 2 h where they received all their water (range, 0.5 to 2 ml). If mice did not maintain a stable body weight, they received supplementary water<sup>21</sup>. All surgical procedures were carried out aseptically under 1–2% isofluorane anaesthesia. Buprenorphine HCl (0.1 mg kg<sup>-1</sup>, intraperitoneal injection; Bedford Laboratories) was used for postoperative analgesia. Ketoprofen (5 mg kg<sup>-1</sup>, subcutaneous injection; Fort Dodge Animal Health) was used at the time of surgery and postoperatively to reduce inflammation. After the surgery, mice were allowed to recover for at least 3 days with free access to water before water restriction.

**Behaviour.** Mice were prepared for photostimulation and electrophysiology by implantation of a clear skullcap and a headpost<sup>13</sup>. The scalp and periosteum over the dorsal surface of the skull were removed. A layer of cyanoacrylate adhesive (Krazy glue, Elmer's Products Inc.) was directly applied to the intact skull. A custom made headpost<sup>21</sup> was placed on the skull with its anterior edge aligned with the suture lambda (approximately over cerebellum) and cemented in place using clear dental acrylic (Lang Dental Jet Repair Acrylic; part no. 1223-clear). A thin layer of clear dental acrylic was applied over the cyanoacrylate adhesive covering the entire exposed skull, followed by a thin layer of clear nail polish (Electron Microscopy Sciences, part no. 72180).

The behavioural task has been described in detail<sup>13,21</sup>. The stimulus was a metal pin (0.9 mm in diameter), presented at one of two possible positions (Fig. 1). The two pole positions were 4.29 mm apart along the anterior-posterior axis (40° of whisking angle) and were constant across sessions. The posterior pole position was 5 mm from the whisker pad. A two-spout lickport (4.5 mm between spouts) was used to deliver water rewards and record licks. Mouth movements were monitored using a photodiode and an infrared laser diode to obtain reaction time measurements (Thorlabs). High-speed video (Mikrotron Eosens Camera, Norpix, MC1362) was taken over a 11.4 mm × 15.2 mm region at 1 kHz to track the whiskers.

At the beginning of each trial, the vertical pole moved into the plane within reach of the whiskers (0.2 s travel time). The pole remained within reach for 1 s, after which it was retracted (retraction time 0.2 s). Mice made contacts with the object at both pole positions, typically with a different set of whiskers. The sample epoch is defined as the time between the pole movement onset to 0.1 s after the pole retraction onset (sample epoch, 1.3 s total, Fig. 1b). The delay epoch lasted for another 1.2 s after completion of pole retraction (delay epoch, 1.3 s total, Fig. 1b). An auditory go cue indicated the end of the delay epoch (pure tone, 3.4 kHz, 0.1 s duration). Licking early during the trial was punished by a loud alarm sound (siren buzzer, 0.05 s duration), followed by a brief timeout (1–1.2 s). Licking the correct lickport after the go cue led to a small drop of liquid reward (3 µl). Licking the incorrect lickport triggered a timeout (2–5 s). Trials in which mice did not lick within a 1.5 s window after the go cue were rare and typically occurred at the end of a session.

**Viral injection and histology.** To characterize BAC Cre mice we injected eGFP (AAV2/1.CAG.EGFP, <http://www.addgene.com>, plasmid 28014) into one hemisphere and Cre-dependent tdTomato (AAV2/1.CAG.FLEX.tdTomato, UPenn Viral Core, AV-1-ALL864) into ALM on the other hemisphere (Extended Data Fig. 3a). The ALM injection coordinate was 2.5 mm anterior to bregma, 1.5 mm lateral<sup>13</sup>. The injection was made through the thinned skull using a custom, piston-based, volumetric injection system. Glass pipettes (Drummond) were pulled and bevelled to a sharp tip (outer diameter of 30 µm). Pipettes were back-filled with mineral oil and front-loaded with viral suspension immediately before injection. Fifty nanolitres were injected 500 and 800 µm deep. Two weeks post injection, mice were perfused transcardially with PBS followed by 4% paraformaldehyde (PFA)/0.1 M PBS. The brains were fixed overnight and transferred to 20% sucrose before sectioning

on a freezing microtome. Coronal 50 µm free-floating sections were processed using standard fluorescent immunohistochemical techniques. Slide-mounted sections were imaged with a Zeiss microscope, a 10× objective and a Hamamatsu Orca Flash 4 camera. Each coronal section was made up of 80–200 tiles merged with NeuroLucida software<sup>49</sup>. For brainstem injections (Extended Data Fig. 3b, c), 150 nl of a 1:2 mix of AAV2/1.CAG.EGFP and red RetroBeads (Lumafluor) was injected into the intermediate nucleus of the reticular formation (6.65 mm posterior to bregma, 1.25 mm lateral, 4.2–4.5 mm deep) and hypoglossal nucleus, 12N (7.25 mm posterior to bregma, 0 mm lateral, 4–4.25 mm deep). Mice were perfused 4 weeks post injection. The brains sections were imaged on an Olympus Macroscope.

**Photostimulation.** Light from a 473 nm laser (Laser Quantum, part no. Gem 473) or a 594 nm laser (Cobolt Inc., part no. Cobolt Mambo 100) was controlled by an acousto-optical modulator (AOM; Quanta Tech) and a shutter (Vincent Associates). Photostimulation of ALM was performed through the clear skullcap implant by directing the laser over the skull (beam diameter, 400 µm at 4σ). The light transmission through the intact skull is 50%<sup>13</sup>. Photostimulation was deployed on 25% of the behavioural trials. To prevent the mice from distinguishing photostimulation trials from control trials using visual cues, a ‘masking flash’ (40 1 ms pulses at 10 Hz) was delivered using 470 nm LEDs (LUXEON Star) near the eyes of the mice. The masking flash began as the pole started to move and continued through the end of the epoch in which photostimulation could occur.

For silencing we stimulated cortical GABAergic neurons in VGAT-ChR2-EYFP mice, or parvalbumin-positive interneurons in PV-ires-Cre mice crossed to reporter mice expressing ReaChR (Fig. 1). The two methods resulted in similar photoinhibition (data not shown). We used 40 Hz photostimulation with a sinusoidal temporal profile (1.5 mW average power) and a 100 ms linear ramp during the laser offset (this reduced rebound neuronal activity)<sup>13</sup>. The photoinhibition silenced a cortical area of 1 mm radius (at half maximum) through all cortical layers. The temporal onset of the photoinhibition reached its peak within 20 ms of light onset. The photo-inhibition recovered ~100 ms after the onset of the linear ramp<sup>13</sup>. To silence ALM activity during the sample or delay epochs (Fig. 1) we photostimulated for 1.3 s, including the 100 ms ramp, starting at the beginning of the epoch. Thus, photo-inhibition always ended before the response cue.

To activate layer 5 intratelencephalic or pyramidal tract neurons (Fig. 5, Extended Data Figs 6 and 7), we photostimulated the motor cortex in the intratelencephalic or pyramidal tract BAC-Cre driver lines crossed to a Rosa26-ChR2 reporter line (Ai32). During behaviour, we used pulses of light (2 ms pulse duration) at 20 Hz (26 pulses, 1252 ms) and a range of peak powers (1.5, 3, 6, 20 mW). The values reported in the figures indicate the average power (0.06, 0.12, 0.24, 0.8 mW; Fig. 5, Extended Data Figs 3 and 6). In untrained mice, we used 5-ms light pulses and a larger range of peak powers (1.5, 6, 13, 22, 40, 47 mW; average power, 0.15, 0.6, 1.3, 2.2, 4, 4.7 mW; Extended Data Fig. 3).

**Electrophysiology.** A small craniotomy (diameter, 1 mm) was made over ALM one day before the recording sessions<sup>13</sup>. Extracellular spikes were recorded using NeuroNexus silicon probes (part no. A4x8-5mm-100-200-177). The 32 channel voltage signals were multiplexed, recorded on a PCI6133 board at 312.5 kHz (National instrument), and digitized at 14 bit. The signals were demultiplexed into the 32 voltage traces, sampled at 19531.25 Hz and stored for offline analyses. Three to eight recordings were made from each craniotomy. Recording depth was inferred from manipulator readings<sup>13</sup>. To minimize brain movement, a drop of silicone gel (3-4680, Dow Corning, Midland, MI) was applied over the craniotomy after the electrode was in the tissue. The tissue was allowed to settle for several minutes before the recording started.

To optogenetically tag ALM intratelencephalic and pyramidal tract neurons during recording, we first infected ALM neurons with ChR2. Cre-dependent ChR2 virus (AAV2/5.hSyn1.FLEX.hChR2.tdTomato, <http://www.addgene.com>, plasmid 41015)<sup>49</sup> was injected into three Rbp4-Cre mice (targeting both layer 5 intratelencephalic and pyramidal tract neurons), four Tlx\_PL56-Cre mice (layer 5 intratelencephalic neuron), and nine Sim1\_KJ18-Cre mice (pyramidal tract neurons). One-hundred-nanolitre volumes were injected 500 and 800 µm deep. We also used two Tlx\_PL56-Cre cross Ai32 transgenic mice for antidromic tagging of intratelencephalic neurons. However, expression of ChR2 in large numbers of neurons in the transgenic mice resulted in highly synchronized activity upon light stimulation, and consequently, difficulty in isolating antidromically activated single units. To photostimulate the axons of pyramidal tract neurons, an optical fibre (Thorlabs, part no. CFML12L05) was implanted into the reticular formation based on stereotaxic coordinates (5.5 mm posterior, 1 mm lateral, 5 mm deep), ipsilateral to the viral injection site. One to four months after the infection and fibre implant, silicon probe recordings were made from the virus injection site. For photostimulation of intratelencephalic neuron axons, photostimulation was through a cranial window over the contralateral ALM. Pairs of laser pulses (1 ms duration, 47–82 mW peak power, separated by 10 ms) were deployed every 500 ms to elicit antidromic responses from ChR2<sup>+</sup> neurons. Occasionally, slightly longer pulse durations were used

(3 or 5 ms). Antidromic responses were seen on one or two recording channels per recording session.

**Two-photon calcium imaging.** To label intratelencephalic cells for imaging, cholera toxin subunit B (CTB; Alexa 647; Molecular probe, Invitrogen, 0.5% in HEPES buffered saline) was injected to the contralateral (right) ALM (2.5 mm anterior, 1.5 mm lateral to bregma, 300 and 600  $\mu\text{m}$  deep, 100 nl per site). For pyramidal tract cells, red RetroBeads (Lumafluor) were injected into the ipsilateral (left) basal pontine nucleus (3.5 mm posterior, 0.4 mm lateral, 5, 5.4, and 5.8 mm below brain surface, 100 nl per site). Window surgery and GCaMP virus injections were carried out 12–34 days after tracer injection. A circular craniotomy ( $\sim 3 \text{ mm}$  diameter) was made above left ALM (centred at 2.5 mm anterior and 1.5 mm lateral to bregma). AAV2/1-syn-GCaMP6s-WPRE virus (UPenn Viral Core, AV-1-PV2824) was diluted two- to sixfold in HEPES buffered saline. Injections were made at three to five locations centred around ALM (separated by  $\sim 400 \mu\text{m}$ ) and at three depths (210/370/530  $\mu\text{m}$ ) for each location ( $\sim 5$ –6 nl per depth). The imaging window was constructed from two layers of microscope coverglass<sup>10</sup> and fixed to the skull using cyanoacrylate glue and dental acrylic. A metal post for head fixation was implanted posterior to the window using dental acrylic. Water restriction started 5–7 days after window surgery. Behavioural training started  $\sim 5$ –7 days after water restriction.

Imaging experiments started after the animals had learned the task (>70% trials correct; typically  $\sim 20$ –30 days after surgery). Images were acquired using a custom-built two-photon microscope equipped with a resonant galvo scanning module (Thorlabs), controlled by ScanImage 4.2 (<http://www.scanimage.org>). The light source was a femtosecond pulsed laser (Coherent). The objective was a 16 $\times$  water immersion lens (Nikon, 0.8 NA, 3 mm working distance). GCaMP6s was excited at 940 nm and images ( $512 \times 512$  pixels,  $400 \mu\text{m} \times 400 \mu\text{m}$  or  $600 \mu\text{m} \times 600 \mu\text{m}$ ) were acquired at 15 Hz. The average excitation power was up to 120 mW for L5 neurons. After functional imaging of a particular  $z$  plane, the laser wavelength was switched to 830 nm to image Retrobead and CTB-647. A small image stack was acquired around the imaging location to allow unambiguous identification of cells that were out of focus. Retrobead and CTB-647 were imaged with Brightline 609/54 (Semrock) and HQ-675/70-2P (Chroma), respectively.

**Behavioural data analyses.** Performance was computed as the fraction of correct reports, excluding the ‘lick early’ trials. Chance performance was 50%. We also separately computed the performance for lick right and lick left trials (Figs 1 and 5). Behavioural effects of photoinhibition (Fig. 1) and photoactivation (Fig. 5) were quantified by comparing the performance under photostimulation with control performance (Figs 1 and 5). Significance of the performance change in each photostimulation condition was determined using bootstrapping to account for variability across mice, sessions and trials. We tested against the null hypothesis that the performance change caused by photostimulation was due to normal behavioural variability. In each round of bootstrapping, we replaced the original behavioural data set with a re-sampled data set in which we re-sampled with replacement from: (1) animals; (2) sessions performed by each animal; and (3) the trials within each session. We then computed the performance change on the re-sampled data set. Repeating this procedure  $10^4$  times produced a distribution of performance changes that reflected the behavioural variability. The  $P$  value of the observed performance change was computed as the fraction of times the bootstrapping produced an inconsistent performance change (for example, if a performance decrease was observed during photostimulation, the  $P$  value is the fraction of times a performance increase was observed during bootstrapping, one-tailed test).

**Electrophysiology data analyses.** The extracellular recording traces were band-pass filtered (300 Hz–6 kHz). Events that exceeded an amplitude threshold (four standard deviations of the background) were subjected to manual spike sorting to extract single units<sup>13</sup>. A total of 1,408 single units were recorded across 99 recording sessions. Most recorded single units were in layer 5a and 5b. Depths were inferred from manipulator depth and calibration experiments<sup>13</sup>. Spike widths were computed as the trough-to-peak interval in the mean spike waveform (Extended Data Fig. 1). Units with spike width <0.35 ms were defined as fast-spiking neurons (124/1,408) and units with spike width >0.45 ms as putative pyramidal neurons (1,245/1,408). This classification was previously verified by optogenetic tagging of GABAergic neurons<sup>13</sup>. Units with intermediate values (0.35–0.45 ms, 39/1,408) were excluded from our analyses. Fast-spiking neurons had higher baseline firing rates and were less selective than putative pyramidal neurons (Extended Data Fig. 1). We concentrated our analyses on the putative pyramidal neurons.

Neurons were further tested for significant trial-type selectivity during the sample, delay or response epochs, using the spike counts from the lick left and lick right trials (two-tailed  $t$ -test,  $P < 0.05$ ; Fig. 2). Neurons that significantly differentiated trial types during any one of the trial epochs were deemed ‘selective’ (912/1,245). Neurons with selectivity during the sample or delay epochs were classified as having ‘preparatory activity’. Neurons with significant selectivity during the response epoch were classified as having ‘peri-movement selectivity’ (Fig. 2c, d). Selective neurons were classified into ‘contra-preferring’ versus ‘ipsi-preferring’, based on their total

spike counts across all three trial epochs (Fig. 2e). To compute selectivity (Fig 2c), we first determined each neuron’s preferred trial type using spike counts from a subset of the trials (10 trials); selectivity is calculated as the spike rate difference between the trial types on the remaining data. We quantified the dynamics of the ALM population response by computing Pearson’s correlation between population response vectors at different times and the population response vector at the onset of the go cue (Fig. 2c, bottom panel). We assumed all neurons were recorded simultaneously (ignoring potential correlations between neurons). To equalize the contributions of individual neurons, each neuron’s response was mean-subtracted and normalized to the variance of its response across the entire trial epoch (computed in time bins of 200 ms). To compute the contra-selectivity (Fig. 3), we took the firing rate difference between the lick right trials and lick left trials for each neuron. These firing rate differences were averaged across the selective neurons. Only trials in which mice correctly reported pole locations were included. Standard errors of the mean were obtained by bootstrapping (Figs 2 and 3). Bootstrapping was also used to evaluate whether contra-preferring neurons were significantly higher in proportion (Fig. 3f, j). The neuronal data set was re-sampled with replacement, and the  $P$  value reflected the fraction of times when more ipsi-preferring neurons were observed (one-tailed test against the null hypothesis that there were more ipsi-preferring neurons).

Seventy-three neurons were antidromically activated by photostimulating pyramidal tract neuron axons, and 134 neurons were antidromically activated by photo-stimulating intratelencephalic neuron axons. These neurons were further tested for collisions in which we looked for absence of antidromic spikes when preceded by spontaneous spikes (Extended Data Fig. 5)<sup>6</sup>. Neurons that passed the collision test were classified as pyramidal tract neurons (45/73) or intratelencephalic neurons (27/134). Neurons that failed the test were classified as pyramidal-tract-activated (22/73) or intratelencephalic-activated (106/134) because they were presumably synaptically-connected to ChR2<sup>+</sup> neurons and intratelencephalic neurons. A few cells could not be tested due to an absence of spontaneous activity (6/73 from pyramidal tract neuron tagging; 1/134 from intratelencephalic neuron tagging) and these neurons were excluded from further analyses. Pyramidal tract neurons and intratelencephalic neurons had shorter mean antidromic spike latencies (pyramidal tract neurons, 2.7 ms; intratelencephalic neurons, 4.6 ms) and smaller temporal jitter (mean s.d. of the antidromic spike latency, pyramidal tract neurons, 0.1 ms; intratelencephalic neurons, 0.2 ms) than the pyramidal-tract-activated (mean latency, 8.3 ms; jitter, 2.8 ms) and intratelencephalic-activated neurons (mean latency, 9.8 ms; jitter, 2.4 ms). However, the latency distributions overlapped and a neuron could not be reliably inferred as being a ChR2<sup>+</sup> neuron based on its response latency alone (Extended Data Fig. 5e, see example in Extended Data Fig. 5b, d). The classification of intratelencephalic neurons and pyramidal tract neurons was further corroborated by the following observations: first, intratelencephalic neurons had longer spike latencies than pyramidal tract neurons, consistent with previous reports of antidromic electrical stimulation in primates and cats<sup>6,31</sup> and the fact that pyramidal tract neurons have myelinated axons and fast conduction velocities. Second, our observed latency values and the estimated conduction velocities (pyramidal tract,  $6.5 \text{ m s}^{-1}$ ; intratelencephalic,  $2.3 \text{ m s}^{-1}$ ) were in agreement with previous measurements from intratelencephalic neurons and pyramidal tract neurons in mice<sup>50,51</sup>. Finally, intratelencephalic neurons showed greater temporal jitter in response to photostimulation than pyramidal tract neurons (Fig. 3h, Extended Data Fig. 5). However, following a conditioning stimulus, the responses of intratelencephalic neurons to a second light pulse (10 ms later) showed less temporal jitter (Extended Data Fig. 5g). This effect has been described for corpus-callosum-projecting intratelencephalic neurons during electrical stimulation in cats<sup>52</sup>.

**Calcium imaging data analyses.** The brain motion was corrected using a line-by-line correction algorithm<sup>10</sup>. Regions of interest (ROIs) corresponding to identifiable cell bodies were selected using a semi-automated algorithm<sup>32</sup>. Individual neurons were visually identified on average fluorescence images as well as a pixel-based response map and a ‘neighborhood correlation map’ (where the brightness of each pixel encodes the correlation of its fluorescent time course to that of its immediate neighbours) that highlight task-related and active cells, respectively<sup>53</sup>. The fluorescence time course of each cell was measured by averaging all pixels within the ROI, with a correction for neuropil contamination<sup>54</sup>. The fluorescence signal of a cell body was estimated as  $F_{\text{cell\_true}}(t) = F_{\text{cell\_measured}}(t) - r \times F_{\text{neuropil}}(t)$ , with  $r = 0.7$ . The neuropil signal  $F_{\text{neuropil}}(t)$  surrounding each cell was measured by averaging the signal of all pixels within a  $\sim 20 \mu\text{m}$  region from the cell centre (excluding all selected cells). To ensure robust neuropil subtraction, only cells that were at least 5% brighter than the surrounding neuropil were included.  $\Delta F/F_0$  was calculated as  $(F - F_0)/F_0$ , where  $F_0$  is the baseline fluorescence signal averaged over a 0.5 s period immediately before the start of each trial.

Task-related neurons were defined as neurons showing significant fluorescence modulation during the task. This was calculated using non-parametric ANOVA (Kruskal–Wallis test) across multiple 0.33 s time bins (five image samples) during

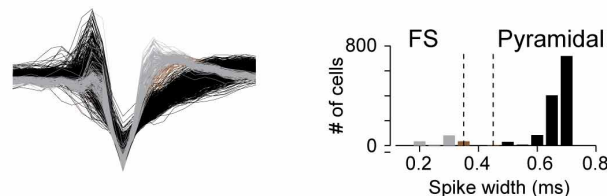
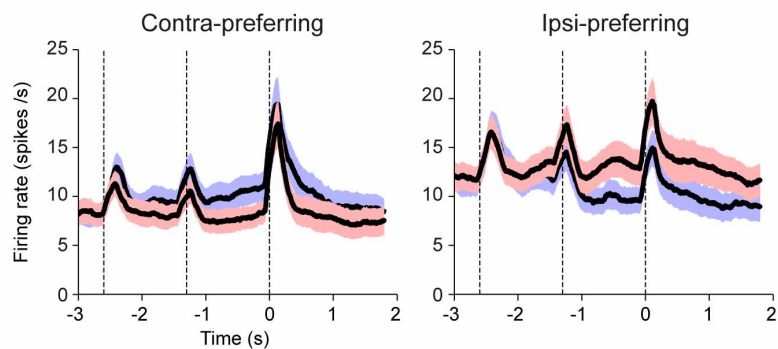
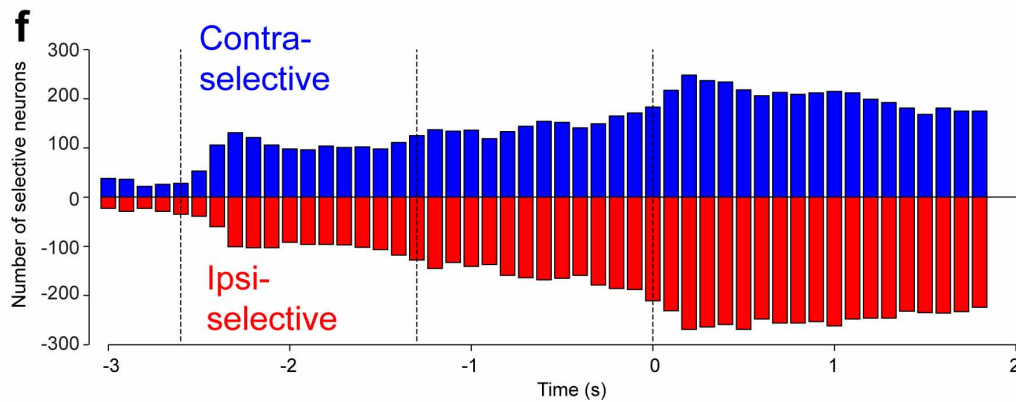
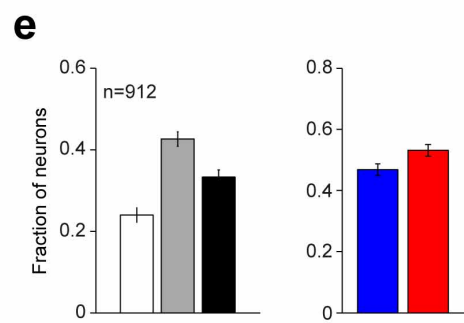
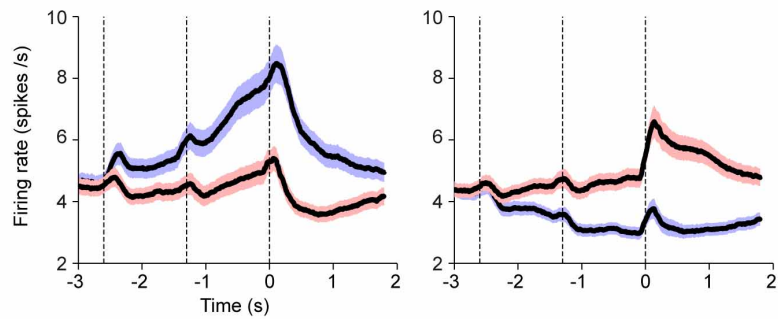
the task. A cell was classified as task-related if the null hypothesis that all time bins had equal fluorescence can be rejected at a *P* value of 0.01 during either contra or ipsi trials. This criterion identified 58% (2,740/4,706) cells as task related. We further defined trial-type-selective cells as a subset of task related neurons that showed significantly different  $\Delta F/F$  response during contra and ipsi trials ( $P < 0.05$ ; Wilcoxon rank sum test). 57% (1575/2740) of task related cell are trial-type selective.

We examined spatial clustering of response types using two different measures. First, we quantified the probability that the nearest neighbour of each contra-preferring or ipsi-preferring cell was of the same response type, compared to the probability calculated by randomly shuffling the response type labels. The *P* value was the fraction of bootstrap trials with probability larger than the observed probability. Second, we quantify the distance between nearest neurons of the same response type and compare the distance to those calculated with randomized response type labels. The *P* value was the fraction of bootstrap trials with distance smaller than the observed distance.

Overall, imaging detected a slight majority of contra-preferring neurons (61%, 971/1,575), whereas no bias was detected based on spike counts (Fig. 2e). To resolve this discrepancy we used spiking data and a model derived from calibration experiments involving simultaneous *in vivo* imaging and recording<sup>32</sup> to simulate fluorescence dynamics (data not shown). The simulations revealed that imaging preferentially detects selectivity in neurons (1) with relatively strong spike rate differences between trial types; (2) responding with an increase, rather than a decrease, in spike rate. Overall this produced a bias for detecting contra-preferring neurons in the simulations, consistent with the observed bias in the imaging experiments. The comparison of simulation and imaging highlights that selectivity evolves differently in contra-preferring and ipsi-preferring neurons (see also Extended Data Fig. 1d). Contra-preferring neurons include a majority of the neurons with large spike count

differences, whereas ipsi-preferring neurons tend to express their selectivity more often through contra-suppression.

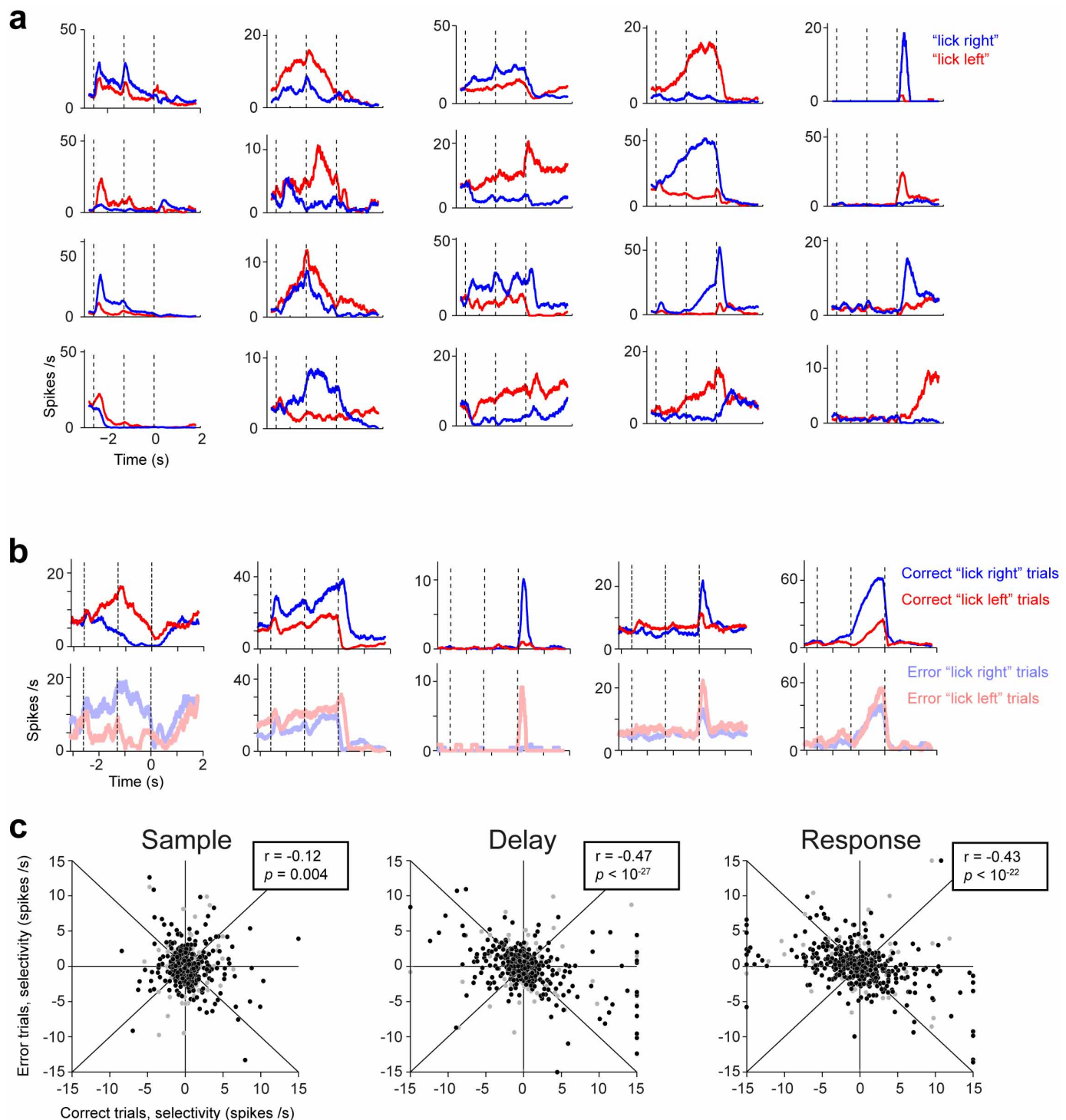
44. Zhao, S. *et al.* Cell type-specific channelrhodopsin-2 transgenic mice for optogenetic dissection of neural circuitry function. *Nature Methods* **8**, 745–752 (2011).
45. Hippenmeyer, S. *et al.* A developmental switch in the response of DRG neurons to ETS transcription factor signaling. *PLoS Biol.* **3**, e159 (2005).
46. Lin, J. Y., Knutson, P. M., Muller, A., Kleinfeld, D. & Tsien, R. Y. ReaChR: a red-shifted variant of channelrhodopsin enables deep transcranial optogenetic excitation. *Nature Neurosci.* **16**, 1499–1508 (2013).
47. Gerfen, C. R., Paletzki, R. & Heintz, N. GENSAT BAC Cre-recombinase driver lines to study the functional organization of cerebral cortical and basal ganglia circuits. *Neuron* **80**, 1368–1383 (2013).
48. Madisen, L. *et al.* A toolbox of Cre-dependent optogenetic transgenic mice for light-induced activation and silencing. *Nature Neurosci.* **15**, 793–802 10.1038/nn.3078 (2012).
49. O'Connor, D. H. *et al.* Neural coding during active somatosensation revealed using illusory touch. *Nature Neurosci.* **16**, 958–965 (2013).
50. Simmons, P. A. & Pearlman, A. L. Receptive-field properties of transcallosal visual cortical neurons in the normal and reeler mouse. *J. Neurophysiol.* **50**, 838–848 (1983).
51. Alstermark, B. & Ogawa, J. In vivo recordings of bulbospinal excitation in adult mouse forelimb motoneurons. *J. Neurophysiol.* **92**, 1958–1962 (2004).
52. Swadlow, H. A., Waxman, S. G. & Rosene, D. L. Latency variability and the identification of antidromically activated neurons in mammalian brain. *Exp. Brain Res.* **32**, 439–443 (1978).
53. Chen, T.-W. *A Systems Level Analysis of Neuronal Network Function in the Olfactory Bulb: Coding, Connectivity, and Modular organization*, PhD Thesis. University of Göttingen, Göttingen, Germany (2008).
54. Kerlin, A. M., Andermann, M. L., Berezovskii, V. K. & Reid, R. C. Broadly tuned response properties of diverse inhibitory neuron subtypes in mouse visual cortex. *Neuron* **67**, 858–871 (2010).

**a Single unit classification****b FS neurons****d Pyramidal neurons**

**Extended Data Figure 1 | Neural selectivity in ALM.** **a**, Single-unit classification. Left, overlaid mean spike waveforms for putative fast-spiking (FS) interneurons (grey,  $n = 124$ ) and putative pyramidal neurons (black,  $n = 1245$ ). A small subset of single units with intermediate spike durations were not classified (brown,  $n = 39$ ). Right, histogram of spike durations (Methods). **b**, Fast-spiking neurons population response (mean  $\pm$  s.e.m.) during the lick right trials (contralateral, blue) and lick left trials (ipsilateral, red). Neurons are sorted by their preferred trial type using spike counts from 10 trials and the

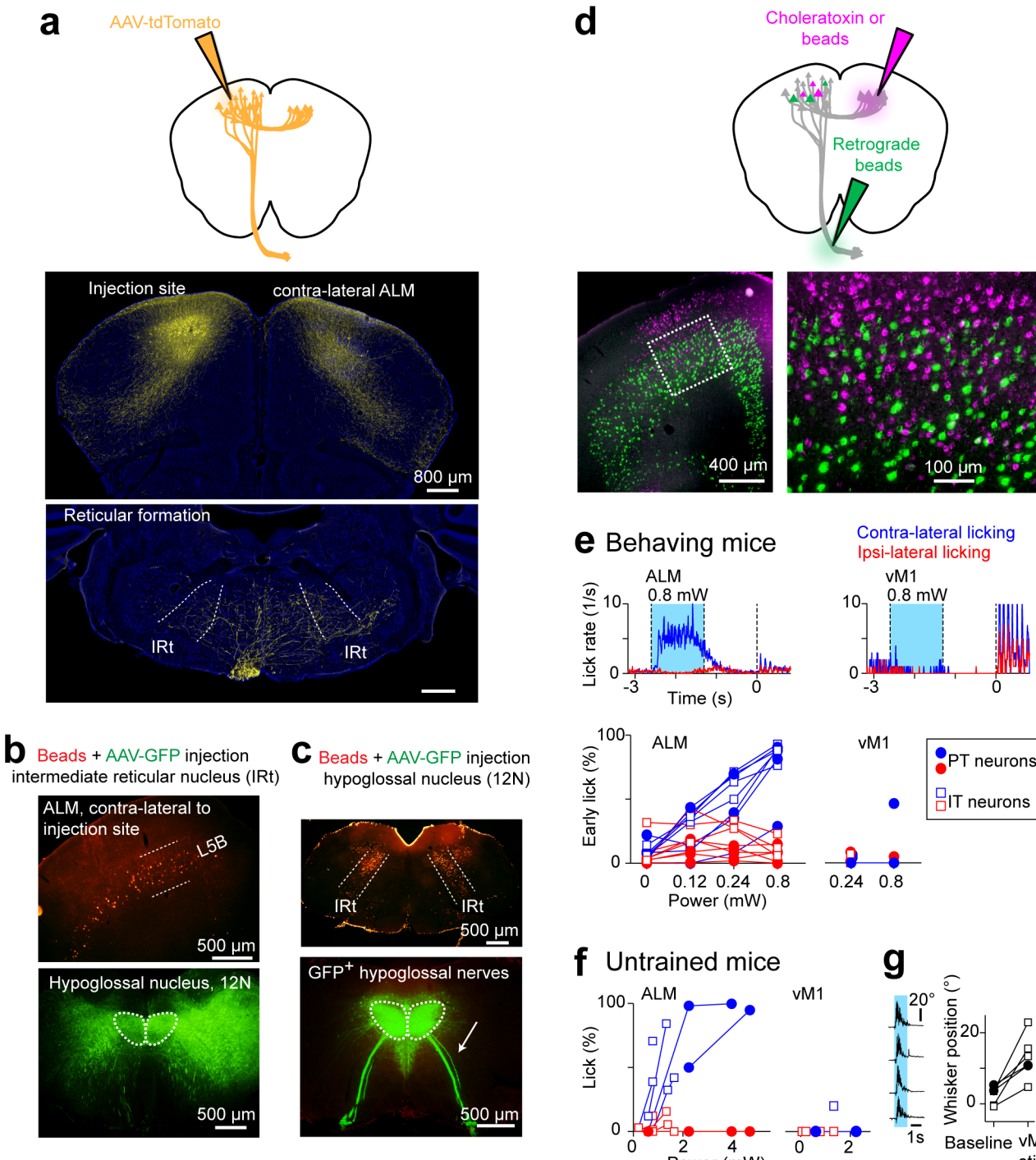
remaining data was used to compute the selectivity. Left, contra-preferring neurons. Right, ipsi-preferring neurons. **c**, Left, proportion of neurons in **b** with preparatory and peri-movement activity. Right, contra-preferring versus ipsi-preferring selectivity. Error bars, s.e.m. across animals, bootstrap.

**d, e**, Same as (**b**) and (**c**) but for putative pyramidal neurons. **f**, Number of significantly selective putative pyramidal neurons as a function of time. Significant selectivity was based on spike counts in 200-ms time windows,  $P < 0.05$ , two-tailed  $t$ -test. Dashed lines, behavioural epochs.



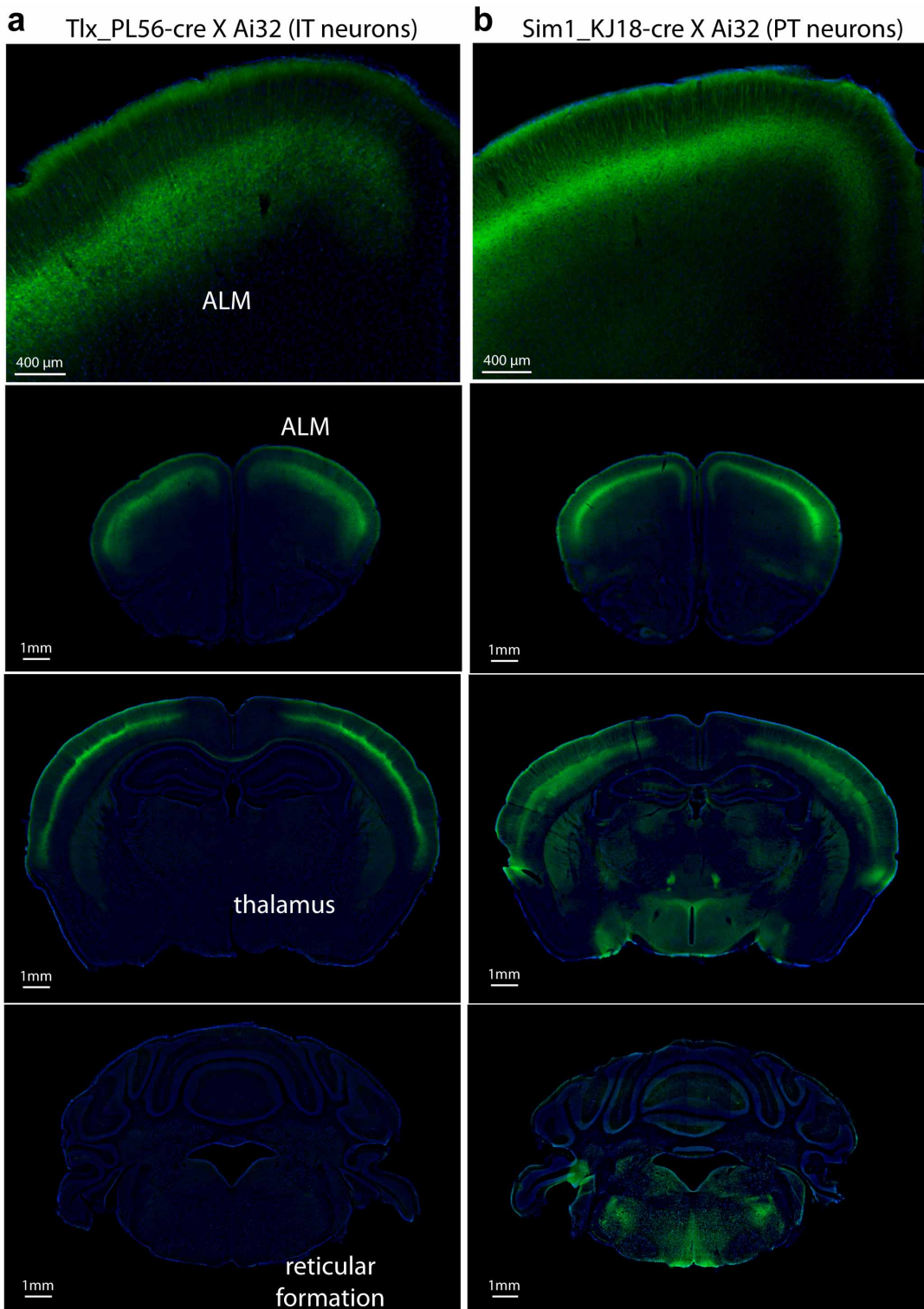
**Extended Data Figure 2 | ALM neurons exhibit temporally complex responses and choice-specific selectivity.** **a**, Twenty example ALM neurons responding during different epochs of the object location discrimination. Correct lick right (blue) and lick left (red) trials only. Dashed lines, behavioural epochs. Averaging window, 200 ms. **b**, Six example ALM neurons during object location discrimination. Top, peri-stimulus time histogram for correct lick right and lick left trials. Bottom, peri-stimulus time histogram for error trials (transparent colour). **c**, ALM neurons show choice-specific preparatory

activity. Selectivity is the firing rate difference between lick right and lick left trials during sample, delay or response epochs ((firing rate lick right)–(firing rate lick left)). Circles, individual neurons ( $n = 912$ ). Filled circles, neurons with significant selectivity ( $P < 0.05$ , two-tailed  $t$ -test). On error trials, when mice licked in the opposite direction to the instruction provided by object location (Fig. 1a), a majority of ALM neurons switched their trial type preference to predict the licking direction, as indicated by the negative correlations ( $r$ , Pearson's correlation).



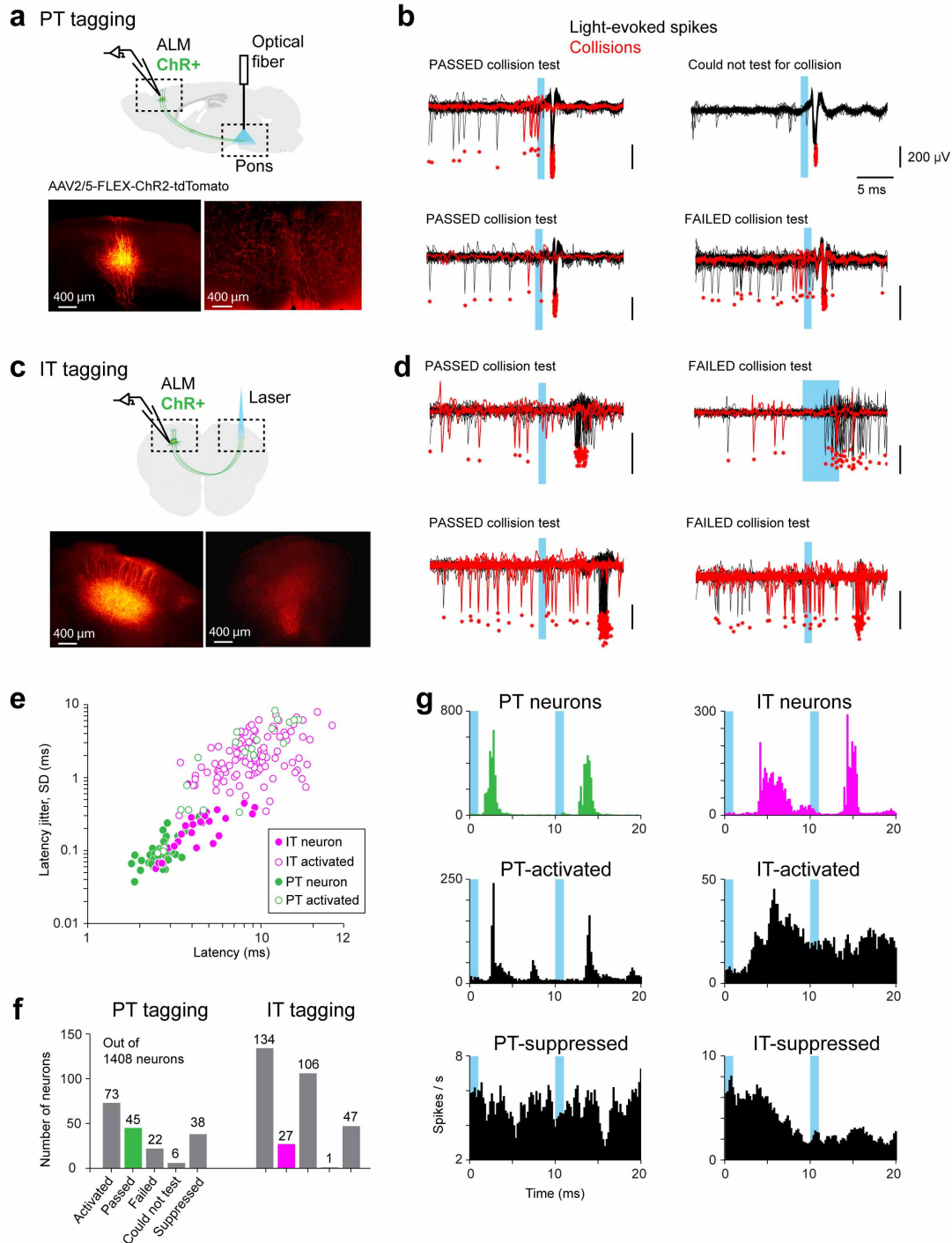
**Extended Data Figure 3 | ALM pyramidal tract neurons control contralateral licking.** **a**, Axonal projections of intratelencephalic neurons (top, Tlx\_PL56 mice) and pyramidal tract neurons (bottom, Sim1\_KJ18 mice). **b**, Top, retrogradely labelled pyramidal tract neurons in contralateral ALM. Bottom, intermediate nucleus of the reticular formation (IRt) axonal projections in the hypoglossal nucleus, 12N. **c**, Top, retrogradely labelled IRt neurons. Bottom, hypoglossal nerves. **d**, Retrograde labelling of pyramidal tract neurons (green) and intratelencephalic neurons (magenta). The ALM coronal slice shows intermingled labelling of pyramidal tract neurons and intratelencephalic neurons without overlap. **e**, Unilateral stimulation of ALM pyramidal tract or intratelencephalic neurons triggered contralateral licking during behaviour (blue, contralateral licking; red, ipsilateral licking). Top, average lick rate during ALM (left) and left vibrissal motor cortex (vM1) (right)

photostimulation,  $n = 8$  mice. Dashed lines, behavioural epochs. Cyan region, photostimulation. Bottom, fraction of trials in which photostimulation caused 'early lick' as a function of laser power. Sample and delay epoch photostimulation data were combined. IT, intratelencephalic; PT, pyramidal tract. **f**, Unilateral stimulation of ALM pyramidal tract or intratelencephalic neurons triggered contralateral licking in untrained mice ( $n = 6$  mice). Fraction of trials in which photostimulation caused licking as a function of laser power. **g**, Unilateral stimulation of left vM1 pyramidal tract or intratelencephalic neurons triggered whisker movements in untrained mice. Left, whisker azimuthal angle traces, individual trials. Right, average whisker angle 500 ms before photostimulation (baseline) and during vM1 photostimulation ( $n = 6$  mice).



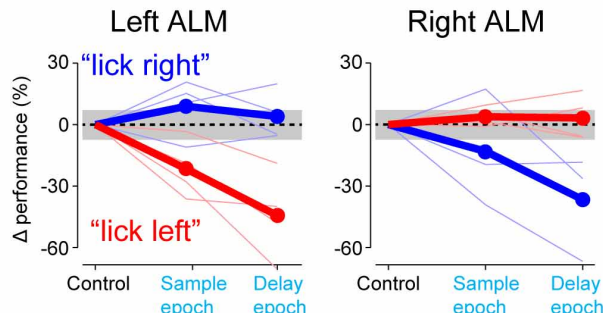
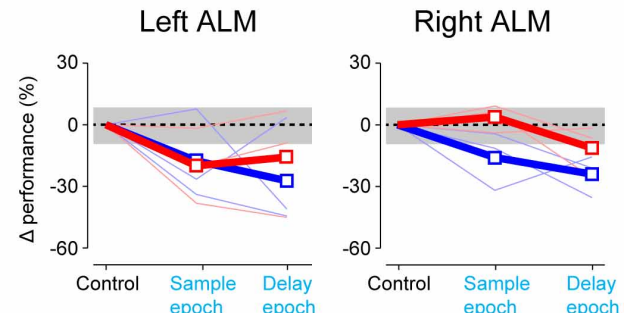
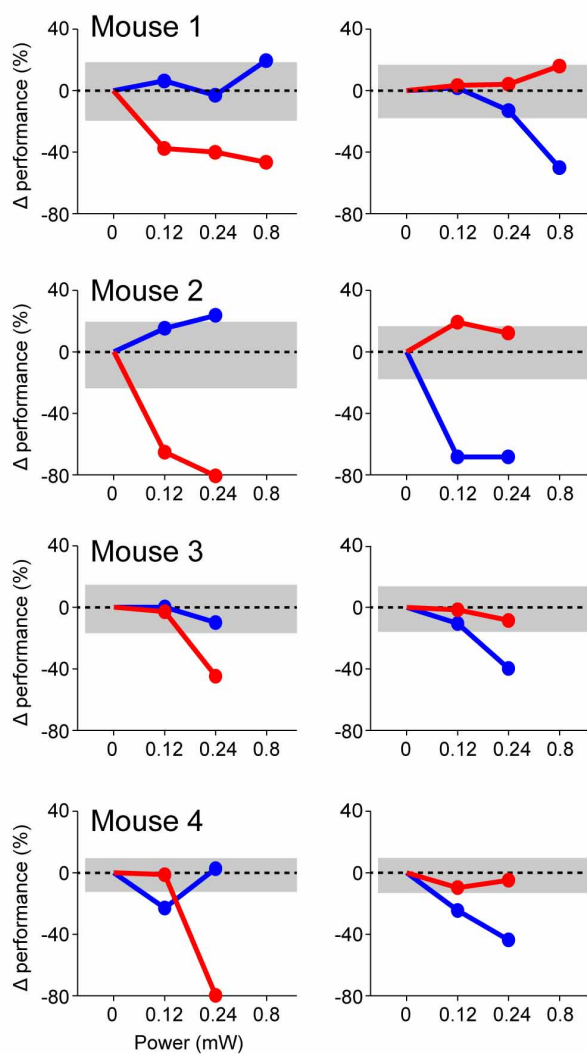
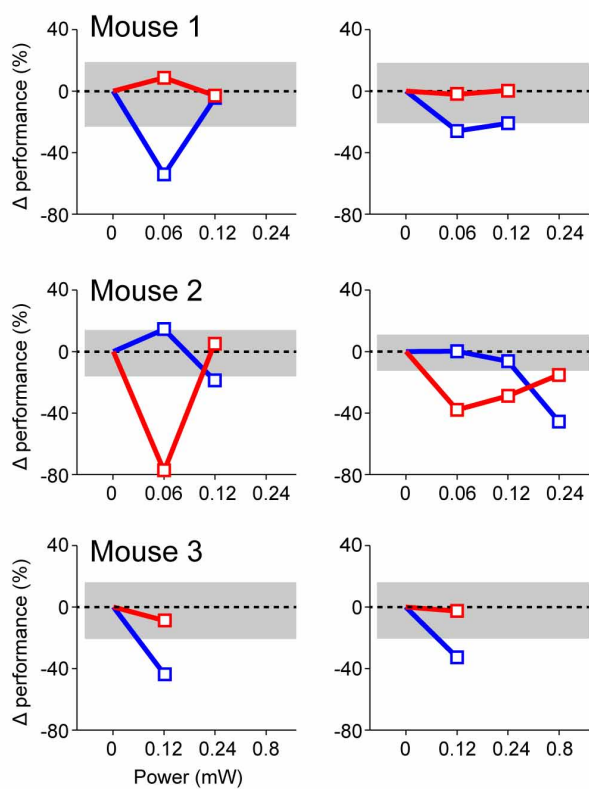
**Extended Data Figure 4 | Transgenic ChR2 expression in intratelencephalic and pyramidal tract neurons.** **a**, ChR2 expression in layer 5 intratelencephalic neurons. Tlx\_PL56-Cre mouse crossed to a Rosa-ChR2-eYFP reporter mouse (Ai32). Top, ChR2 expression in ALM.

Bottom, ChR2 expression in three coronal sections from anterior to posterior. **b**, Same as **a** for ChR2 expression in pyramidal tract neurons. Sim1\_KJ18-Cre mouse crossed to Ai32.



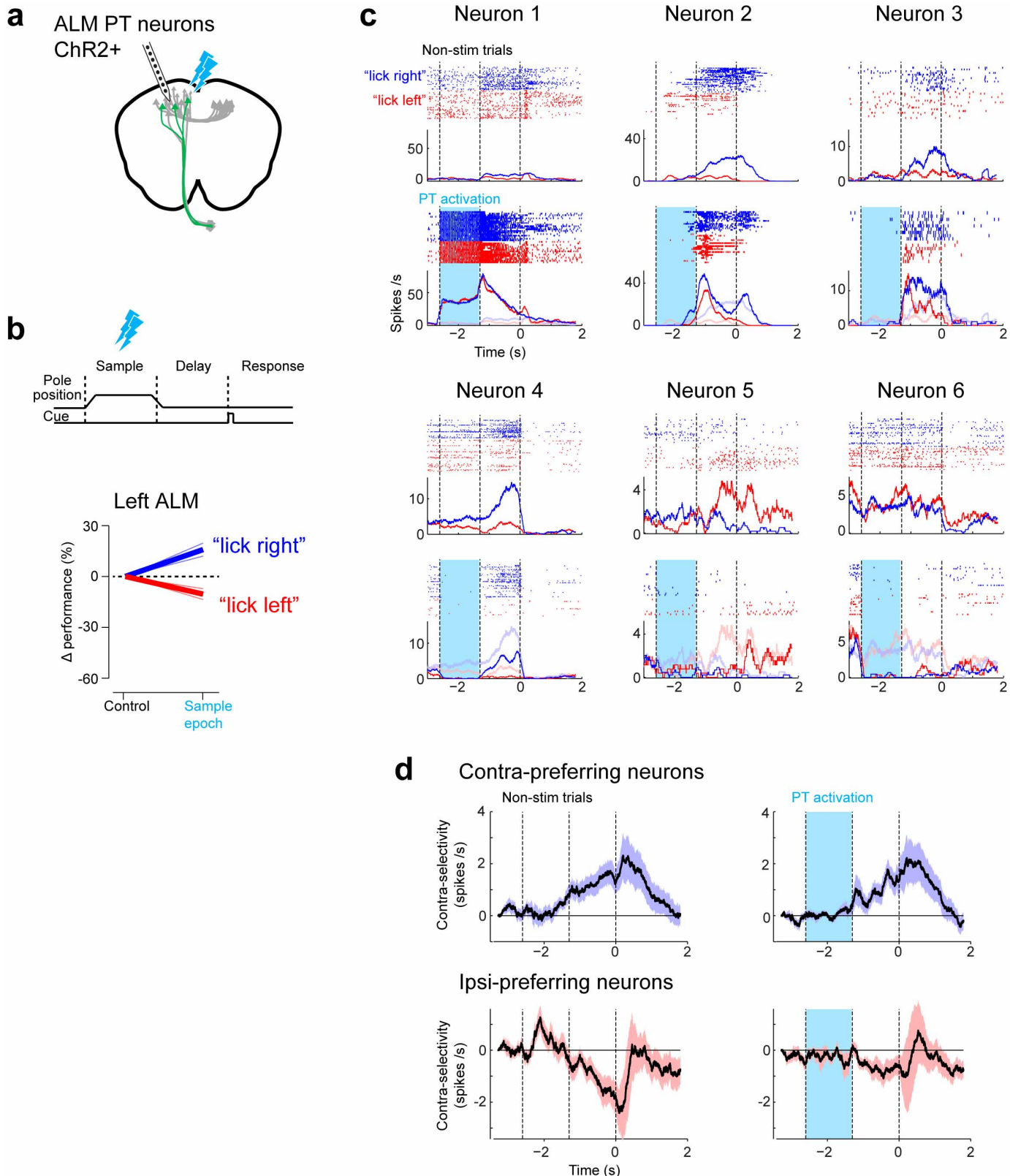
**Extended Data Figure 5 | Cell-type-specific recording with ChR2 tagging.** **a**, Pyramidal tract neuron recordings. Top, left ALM neurons were infected with AAV2/5-FLEX-ChR2-tdTomato (Sim1\_KJ18-Cre mice). An optical fibre was implanted into the left (ipsilateral) reticular formation to antidromically stimulate the pyramidal tract neuron axons. Pyramidal tract neurons were identified based on back-propagating antidromic spikes (tagging). Bottom, expression of ChR2-tdTomato in left ALM; injection site (left), axon terminals in the reticular formation (right). **b**, Recording traces for four example neurons activated by antidromic stimulation of pyramidal tract neurons (blue). Red ticks, individual spikes. Red traces, collision tests. Left, two pyramidal tract neurons that passed the collision test; antidromic spikes were absent when preceded by spontaneous spikes. These neurons were classified as pyramidal tract neurons. Right, two neurons that failed the collision test. The top neuron could not be tested for collision due to an absence of baseline firing. The bottom neuron failed the collision test because light-evoked spikes occurred even when preceded by spontaneous spikes. This neuron was classified as a

pyramidal-tract-activated neuron. Scale bars, 200 μV, 5 ms. **c, d**, Same as **a** and **b** but for intratellencephalic neuron recordings. **e**, Antidromic spike latency versus jitter (SD) for pyramidal tract neurons, intratellencephalic neurons, pyramidal-tract-activated neurons, and intratellencephalic-activated neurons. **f**, Recording yield. ‘Activated’, neurons activated by antidromic stimulation; ‘Passed’, subsets of activated neurons that passed the collision test. These neurons were classified as pyramidal tract neurons or intratellencephalic neurons. ‘Failed’, subsets of activated neurons in which spontaneous spikes failed to block light-evoked spikes. ‘Could not test’, the subset of activated neurons without spontaneous activity. These neurons were excluded from analyses. ‘Suppressed’, neurons suppressed by antidromic stimulation. **g**, Top, light-evoked responses across all pyramidal tract neurons and intratellencephalic neurons. Middle, pyramidal-tract-activated neurons and intratellencephalic-activated neurons. Bottom, pyramidal-tract-suppressed neurons and intratellencephalic-suppressed neurons.

**a Activate PT neurons (Sim1\_KJ18-cre x Ai32)****c Activate IT neurons (Tlx\_PL56-cre x Ai32)****b Delay epoch photostimulation****d**

**Extended Data Figure 6 | Photostimulation of intratelencephalic and pyramidal tract neurons biases upcoming licking direction.** **a**, Performance change, pyramidal tract neurons activation. Re-plot of the data in Fig. 5b. Grey areas represent 95% confidence interval of expected behavioural variability. We estimated the behavioural variability by computing performance changes on re-sampled data sets in which we sampled with

replacement from only the control trials (Methods, repeated  $10^4$  times). The number of trials in the re-sampled data sets was matched to the actual experiments. **b**, Dose response for individual mouse in **a**. Delay epoch photostimulation data only. **c, d**, Same as **a** and **b** but for intratelencephalic neurons activation.



**Extended Data Figure 7 | Photostimulation of pyramidal tract neurons during the sample epoch causes persistent changes in ALM activity and a directional bias.** **a**, Simultaneous recordings and photostimulation of left ALM pyramidal tract neurons during behaviour. Two mice, eight sessions, 91 neurons. **b**, Stimulation of left ALM pyramidal tract neurons during the sample epoch biased the upcoming licking to the contralateral direction. Top, sample epoch photostimulation. Bottom, performance change relative to the control trials. Thick lines, mean; thin lines, individual mice. **c**, Spike raster plots and peri-stimulus time histograms of six example neurons. Correct lick

right (blue) and lick left (red) trials only. Dashed lines, behavioural epochs. For each neuron: top, control trials; bottom, photostimulation trials (solid colour). Control trials are overlaid in transparent colour. Averaging window, 200 ms. **d**, Average population selectivity (black line,  $\pm$ s.e.m. across neurons). Left, control trials. Right, photostimulation trials. Neurons are sorted by their preferred trial type (top, contra-preferring neurons; bottom, ipsi-preferring neurons). Selectivity is the difference in spike rate between the preferred and non-preferred trial type.